

## An Ionic Lock Mediates Interdomain Interactions in G protein $\alpha_i$ subunits and Determines $G\alpha_i$ Subtype Signaling Specificity

Tyler J. Lefevre<sup>1,2</sup>, Wenyuan Wei<sup>4†</sup>, Elizaveta Mukhaleva<sup>4†</sup>, Sai Pranathi Meda Venkata<sup>1</sup>, Naincy Chandan<sup>1,3</sup>, Saji Abraham<sup>1</sup>, Nagarajan Vaidehi<sup>4</sup>, and Alan V. Smrcka<sup>1\*</sup>

<sup>1</sup>Department of Pharmacology, University of Michigan Medical School, Ann Arbor, MI; <sup>2</sup>Program in Chemical Biology, University of Michigan, Ann Arbor, MI; <sup>3</sup>Genentech, South San Francisco, CA; <sup>4</sup>Department of Computational and Quantitative Medicine, Beckman Research Institute of the City of Hope, Duarte, CA

\*Correspondence:

Alan V. Smrcka, Ph.D.

Email: [avsmrcka@umich.edu](mailto:avsmrcka@umich.edu)

Phone: 734-615-4945

†These authors contributed equally.

## Abstract

Highly homologous members of the  $G\alpha_i$  family,  $G\alpha_{i1-3}$ , have distinct tissue distributions and physiological functions, yet the functional properties of these proteins with respect to GDP/GTP binding and regulation of the canonical effector adenylate cyclase are very similar. We recently identified PDZ-RhoGEF (PRG) as a novel  $G\alpha_{i1}$  effector, however, it is poorly activated by  $G\alpha_{i2}$ . Here we investigated the mechanistic basis for this selectivity using PRG as a representative target. We find that substitution of either the helical domain (HD) from  $G\alpha_{i1}$  into  $G\alpha_{i2}$  or substitution of a single amino acid, A230 in  $G\alpha_{i2}$  to the corresponding D in  $G\alpha_{i1}$ , largely rescues PRG activation and interactions with other  $G\alpha_i$  targets identified in a proteomic screen. Molecular dynamics simulations combined with Bayesian network models revealed that in the GTP bound state, dynamic separation at the HD-Ras-like domain (RLD) interface is prevalent in  $G\alpha_{i2}$  relative to  $G\alpha_{i1}$  and that mutation of A230<sup>S4h3.3</sup> to D in  $G\alpha_{i2}$  stabilizes HD-RLD interactions through formation of an ionic interaction with R145<sup>HD.11</sup> in the HD. These interactions in turn modify the conformation of Switch III. These data support a model where D229<sup>S4h3.3</sup> in  $G\alpha_{i1}$  interacts with R144<sup>HD.11</sup> stabilizes a network of interactions between HD and RLD to promote protein target recognition. The corresponding A230 in  $G\alpha_{i2}$  is unable to form the “ionic lock” to stabilize this network leading to an overall lower efficacy with respect to target interactions. This reveals significant distinct mechanistic properties that could underly the differential biological and physiological consequences of activation of  $G\alpha_{i1}$  or  $G\alpha_{i2}$  by GPCRs.

## **Introduction**

Many physiologically important hormones and neurotransmitters signal through G protein-coupled receptors (GPCRs), rendering these membrane-spanning receptors highly clinically significant as important drug targets<sup>1,2</sup>. GPCRs transduce signals into the cell via heterotrimeric G proteins, consisting of the  $G\alpha$  subunit and the  $G\beta\gamma$  constitutive heterodimer. Signaling diversity from GPCRs is primarily achieved via an array of  $G\alpha$  subunit protein families which harbor distinct downstream signaling capabilities, including the  $G_s$ ,  $G_{i/o}$ ,  $G_{q/11}$ , and  $G_{12/13}$  families<sup>3-6</sup>.

$G\alpha$  subunits consist of a Ras-like domain (RLD), which binds and hydrolyzes guanine nucleotides, and an all-helical domain (HD), connected by a flexible hinge region<sup>5,7</sup>. Much of the investigative focus on  $G\alpha$  protein function has been on the RLD, which harbors three “Switch” regions (Switch I-III) that undergo conformational alterations upon GTP binding. Upon binding GTP, Switch regions I-III collapse toward the bound nucleotide in a conformational rearrangement that permits  $G\alpha$ ·GTP-effector interaction after separation from  $G\beta\gamma$  and the receptor<sup>8</sup>. In contrast, the HD is relatively rigid and opens along the interdomain cleft via the flexible hinge in the nucleotide free transition state along the pathway of receptor-mediated GDP release<sup>9-11</sup>. Mutation of residues along the Ras-HD interface further increases receptor-independent rate of GDP dissociation in  $G\alpha_i$ <sup>12</sup>.

Generally, the  $G\alpha_s$  family activates adenylyl cyclases (ACs) to produce 3',5'-cyclic adenosine monophosphate (cAMP) and the  $G\alpha_i$  family inhibits ACs<sup>3</sup>. The  $G\alpha_{i/o}$  family consists of  $G\alpha_{i1}$ ,  $G\alpha_{i2}$ ,  $G\alpha_{i3}$ ,  $G\alpha_o$ ,  $G\alpha_{T1}$ ,  $G\alpha_{T2}$ ,  $G\alpha_{T3}$ , and  $G\alpha_z$ .  $G\alpha_o$  is prominent in the brain,  $G\alpha_T$  in the visual and taste systems, and  $G\alpha_z$  in the brain and prostate.  $G\alpha_{i2}$

protein expression is more widespread and more abundant than any other protein in the  $G\alpha_{i/o}$  family, except for  $G\alpha_o$  <sup>13</sup>.  $G\alpha_{i1-3}$  are expressed broadly in humans, with  $G\alpha_{i2}$  often being expressed alongside  $G\alpha_{i3}$  and/or  $G\alpha_{i1}$ .  $G\alpha_{i1-3}$  subunits are 94% identical between  $G\alpha_{i1}$  and  $G\alpha_{i3}$ , 86% identical between  $G\alpha_{i1}$  and  $G\alpha_{i2}$ , and 88% identical between  $G\alpha_{i2}$  and  $G\alpha_{i3}$  <sup>14</sup>. These three members of the  $G\alpha_i$  subfamily have identical rates of single turnover GTP hydrolysis, but the GDP dissociation rate from  $G\alpha_{i2}$  is approximately two-fold faster than for the other two isoforms <sup>15</sup>.

In terms of signaling specificity, all  $G\alpha_i$  subtypes inhibit various AC isoforms with similar potency and efficacy <sup>16</sup>. For decades, AC was the only known effector of  $G\alpha_i$ . Subsequently, a small number of proteins have been characterized as binding partners of  $G\alpha_i$ : G protein-activated inwardly-rectifying potassium channels (GIRK) <sup>17-20</sup> <sup>21</sup>, epidermal growth factor receptor (EGFR), and growth factor receptor binding 2-associated binding protein 1 (Gab1) <sup>22</sup>, although the biochemical and biological significance of these interactions is less well understood.

Importantly, genetic deletion or inactivation of endogenous individual  $G\alpha_i$  isoforms have yielded evidence for differential function in primary tissues and organisms. For example, knockout of  $G\alpha_{i2}$  in mice results in exacerbated ischemic injury and cardiac infarction, while mice lacking  $G\alpha_{i3}$  saw an upregulation in  $G\alpha_{i2}$  and reduced injury <sup>21,23-26</sup>. Additionally,  $G\alpha_{i2}$  primarily promotes arrest and  $G\alpha_{i3}$  is required for transmigration and chemotaxis in mouse neutrophils <sup>27</sup>, while  $G\alpha_{i3}$  activation downstream of CXCR3 has been shown to inhibit  $G\alpha_{i2}$  activation in murine activated T cells <sup>28</sup>. These data strongly suggest that these isoforms serve non-redundant, unique functions, yet the biochemical

basis for driving selective functionality has yet to be determined despite nearly three decades of research.

Recently, our laboratory identified PDZ-RhoGEF (PRG) as a novel, direct effector of  $G\alpha_i$  in an unbiased proximity interaction screen<sup>29</sup>.  $G\alpha_{i1}$  binds and activates PRG in a nucleotide-dependent and receptor-dependent manner in cells.  $G\alpha_{i3}$  also activates PRG, but  $G\alpha_{i2}$  only weakly stimulates PRG. Here, we have interrogated the nature of the specificity of  $G\alpha_i$  subfamily members for PRG at the molecular level. In doing so, we have uncovered an atomic-level mechanism where the differences between  $G\alpha_{i1}$  and  $G\alpha_{i2}$  with respect to the ability to stabilize interactions between the HD and the Switch III region of the RLD results in weaker PRG engagement by  $G\alpha_{i2}$ . Follow-up with unbiased proximity labeling coupled to tandem MS proteomics supports the idea that this mechanism extends beyond PRG interactions to multiple additional  $G\alpha_i$  targets. Overall, our studies support a model in which the strength and frequency of interactions between  $G\alpha_i$  Switch III and the HD control the ability to bind and activate PRG and other target proteins, differentiating  $G\alpha_i$  subfamily structure and function.

## **Results**

### **G $\alpha_{i1}$ more effectively activates and interacts with PRG than G $\alpha_{i2}$**

We have previously shown<sup>29</sup> that G $\alpha_{i1}$  stimulates PRG and subsequent RhoA activation in a manner dependent on the activation state of G $\alpha_i$ . To mimic that GTP bound state of G $\alpha_i$ , a catalytic glutamine 204 was substituted with leucine which strongly inhibits GTP hydrolysis leading to constitutive GTP binding and activation<sup>7,30-32</sup>. Transient co-expression of G $\alpha_{i1}$  Q204L (G $\alpha_{i1}$  QL), PRG, and an SRE-luciferase plasmid that reports on RhoA activation in HEK293 cells (Fig. 1A) results in significant PRG activation (Fig. 1B). G $\alpha_{i2}$  Q205L (G $\alpha_{i2}$  QL) only weakly activates PRG activity in the same assay. Concentration-response experiments show a significant difference in the efficacy of PRG activation by G $\alpha_{i1}$  QL and G $\alpha_{i2}$  QL (Fig. 1C). This indicates that the difference is not due to differences in GTP binding since this would alter the potency of activation rather than efficacy. There is some variability in this assay with respect to the fold activation of PRG by G $\alpha_i$  but the differences between G $\alpha_{i1}$  and G $\alpha_{i2}$  remain internally consistent within each assay set.

To validate PRG-G $\alpha_i$  interactions in cells, we performed a NanoBiT nanoluciferase complementation assay<sup>33</sup>, in which the NanoLuc LgBiT was inserted after the  $\alpha$ A helix in G $\alpha$  subunits<sup>34</sup>, and NanoLuc SmBiT was appended to the prior to the N-terminal Myc tag of myc-PRG (Fig. 1D). Coexpressing G $\alpha_{i1}$  QL-LgBiT constructs with SmBiT-PRG in HEK293 cells resulted in an increase in luminescent signal relative

to  $G\alpha_{i1}$  WT-LgBiT, indicating a nucleotide-dependent interaction with PRG. This was not observed for QL variants in  $G\alpha_{i2}$ ,  $G\alpha_s$ , or  $G\alpha_q$  (Fig. 1E). Together, these results show that  $G\alpha_{i1}$  interacts with, and activates PRG in a GTP-dependent manner, while  $G\alpha_{i2}$  is much less efficient in this interaction.

### **Active $G\alpha_{i2}$ QL BioID weakly engages the proximal interactome relative to $G\alpha_{i1}$ QL BioID**

Given their previously known functional overlap, the stark disparity between  $G\alpha_{i1}$  and  $G\alpha_{i2}$  in their ability to activate PRG prompted us to probe for further examples of selectivity between  $G\alpha_i$  subtypes. PRG was initially identified as a novel target of  $G\alpha_{i1}$  using unbiased BioID2 proximity labeling coupled to mass spectrometry. BioID2 functionalizes biotin releasing reactive biotinoyl-5'-AMP, which biotinylates proximal lysines within 20 nm<sup>35</sup>. By comparing relative biotinylation by BioID2 fused to either  $G\alpha_i$  WT or  $G\alpha_i$  QL, we revealed the activated  $G\alpha_i$  proximity interactome. Here, we applied this approach to probe the relative interactomes of  $G\alpha_{i1}$  and  $G\alpha_{i2}$ .

Briefly, HA- $G\alpha_{i1}$  Q204L-BioID2 ( $G\alpha_{i1}$  QL-BioID), HA- $G\alpha_{i2}$ -BioID2 ( $G\alpha_{i2}$ -BioID), and HA- $G\alpha_{i2}$  Q205L-BioID2 ( $G\alpha_{i2}$  QL-BioID) were transiently transfected into HT1080 fibrosarcoma cells and incubated with biotin to allow labeling of proximal proteins by  $G\alpha_i$ -BioID. After 24 hours of protein expression and biotin labeling, cells were lysed, biotinylated proteins were captured with streptavidin beads, and labeled with isobaric tandem mass tag (TMT) labels. Samples from all experimental groups were then analyzed via LC MS/MS in a single run (Fig. 2A). Proteins statistically significantly enriched in QL vs WT samples are considered proximal interactors. Volcano plots were generated for all the proteins identified with the statistical cutoffs for significance from

two different comparisons,  $G\alpha_{i1}$  QL/ $G\alpha_{i2}$  WT (Fig. 2B top panel) and  $G\alpha_{i2}$  QL/ $G\alpha_{i2}$  WT (Fig. 2B bottom panel). We assumed that the  $G\alpha_i$  WT interactions would be similar between the two subtypes thus  $G\alpha_{i2}$  was used as a baseline for both plots. Validation of this assumption is discussed below.

The identities and fold QL/WT enrichment levels for many hits for active  $G\alpha_{i1}$ -BioID were consistent with those found in our previous screen<sup>29</sup>. Notably, there are no significant observable differences in identity of most of the proteins enriched for interaction with active  $G\alpha_{i1}$  QL-BioID vs  $G\alpha_{i2}$  QL-BioID. However, the number of proteins identified that reached statistical significance [ $-\log(\text{abundance ratio p-value}) \geq 2.0$ ] were markedly fewer in  $G\alpha_{i2}$  QL-BioID2 samples than in  $G\alpha_{i1}$  QL-BioID2 samples. This is largely because the  $G\alpha_{i2}$  QL-BioID2 /  $G\alpha_{i2}$  WT-BioID2 fold enrichment was generally lower than for  $G\alpha_{i1}$  QL BioID2. These data indicate a difference in overall signaling activity of  $G\alpha_{i1}$ -GTP compared to  $G\alpha_{i2}$ -GTP.

To confirm that these observations are not an artifact of the mass spectrometry analysis and that using  $G\alpha_{i2}$  WT as a baseline in both plots is valid, verification assays were performed with selected “hits” that showed significant differences between  $G\alpha_{i1}$  QL and  $G\alpha_{i2}$  QL engagement. Epitope-tagged mammalian expression constructs were transiently co-expressed in HEK293 cells with either  $G\alpha_{i1}$ -BioID,  $G\alpha_{i1}$  QL-BioID2,  $G\alpha_{i2}$ -BioID2,  $G\alpha_{i2}$  QL-BioID2, or membrane-targeted BioID2 (BioID2-CAAX). Exogenous biotin was added for 24 hours, followed by a lysis and streptavidin bead purification. Captured biotinylated protein samples were run on SDS-PAGE and analyzed for pulldown via western blotting using antibodies against the respective affinity tags for the target proteins.



Proteins selected for analysis included several targets that were found in our previous report<sup>29</sup> and represent diverse signaling pathways: PDZ-RhoGEF,  $\alpha$ -Parvin (Parvin), Vimentin, Ribosomal protein S6 Kinase A1 (RSK1), Neurofibromin 1 (NF1), and Ras p21 protein activator 2 (RASA2). Proteins including NF1, PRG, and Parvin showed selective enrichment in  $G\alpha_{i1}$  QL/WT over  $G\alpha_{i2}$  QL/WT (Fig. 2C). Vimentin and RASA2 showed only a slight preference for interaction with  $G\alpha_{i1}$  QL-BioID over  $G\alpha_{i2}$  QL-BioID, while RSK1 did not preferentially interact with either  $G\alpha_{i1}$  QL-BioID or  $G\alpha_{i2}$  QL-BioID over the WT-BioID variants. These results indicate that many of the proximal interactors found in the proteomic screen are reproducible in an orthogonal assay and are suitable for further analysis in their relationship to  $G\alpha_i$ . Importantly, the results confirm that nucleotide-dependent interaction with these targets by  $G\alpha_{i2}$  is weaker than for  $G\alpha_{i1}$ .

### **Substitution of the $G\alpha_{i1}$ helical domain (HD) into $G\alpha_{i2}$ is sufficient to confer activation of PRG**

To understand the molecular determinants that drive specificity of activation of PRG by  $G\alpha_{i1}$ , and perhaps by extension other targets, we mapped the amino acid differences between the  $G\alpha_i$  subfamily onto a crystal structure of  $G\alpha_{i1}$  bound to a GTP analogue, GPPNHP (PDB 1CIP). We previously reported that  $G\alpha_{i3}$  activates PRG, so we highlighted amino acids homologous between  $G\alpha_{i1}$  and  $G\alpha_{i3}$  but different from  $G\alpha_{i2}$  (33 residues) (Fig. 3A). The helical domain (HD) of  $G\alpha_i$  shows the region of greatest divergence between  $G\alpha_i$  subtypes (Figs. 3A and 4A), containing 21 of the differences between  $G\alpha_{i1}/G\alpha_{i3}$  and  $G\alpha_{i2}$ . As an initial approach, we substituted the entire HD of  $G\alpha_{i1}$  (residues 62-167) into the corresponding position in  $G\alpha_{i2}$ , resulting in the chimeric  $G\alpha_i$

protein  $G\alpha_{i2}$ -1HD (Fig. 3B). This chimera is expressed in HEK293 cells and functionally inhibits forskolin-dependent cAMP generation by adenylyl cyclase (Fig. S1A and B).  $G\alpha_{i2}$ -1HD or  $G\alpha_{i2}$ -1HD Q205L (QL) were then transfected into HEK293 cells in the SRE-luciferase reporter assay to examine their ability to activate PRG. Strikingly,  $G\alpha_{i2}$ -1HD QL expression results in strong activation of PRG as compared to  $G\alpha_{i2}$  QL (Fig. 3C), indicating that the HD of  $G\alpha_{i1}$ , when substituted into  $G\alpha_{i2}$ , is sufficient to confer nucleotide-dependent activation of PRG.

To try to identify structural elements within the  $G\alpha_{i1}$  HD that confer PRG activation, the HD was subdivided into three segments consisting of 1) The  $G\alpha$   $\alpha$ A helix, 2)  $\alpha$ B –  $\alpha$ C helices, and 3)  $\alpha$ D –  $\alpha$ E helices. Each of these subdivisions of the  $G\alpha_{i1}$  HD were then substituted into their cognate positions in  $G\alpha_{i2}$  (Fig. 3B). Neither the  $\alpha$ A helix nor the  $\alpha$ B- $\alpha$ C helix subdivisions of  $G\alpha_{i1}$ , when substituted into  $G\alpha_{i2}$ , activate PRG in cells more than  $G\alpha_{i2}$  Q205L (Fig. 3D), but inhibited cAMP generation by adenylyl cyclase (Fig. S1C). The  $\alpha$ D- $\alpha$ E substitution was deficient in the cAMP inhibition assay and could not be analyzed. These data suggest that  $G\alpha_{i1}$ -mediated activation of PRG relies on some intrinsic property of the intact  $G\alpha_{i1}$  HD rather than one residue or a subset of residues within the  $G\alpha_{i1}$  HD. It is possible that the  $G\alpha_{i1}$  HD participates in direct binding interactions with PRG but may also confer specificity through interactions with of some component of the RLD in  $G\alpha_i$ .

The striking increase in PRG activation observed with substitution of the  $G\alpha_{i1}$  HD into  $G\alpha_{i2}$  prompted us to test the interaction of these  $G\alpha_{i2}$  variants with other protein targets from the BiID proximity labeling screen. We tested multiple targets for activation-dependent labeling using the proximity labeling-dependent western blotting

assay with the WT and QL versions of  $G\alpha_{i1}$ ,  $G\alpha_{i2}$  and  $G\alpha_{i2}$ -1HD (Fig. 3E, S1E). The western blots comparing  $G\alpha_{i1}$ -BioID2 and  $G\alpha_{i2}$ -BioID2 are the same as in Fig. 2 but here we included results with  $G\alpha_{i2}$ -1HD-BioID2 for comparison. Substitution of the  $G\alpha_{i1}$  HD into  $G\alpha_{i2}$  partially rescues the QL-dependent labeling of some of these targets. Parvin shows the most striking rescue while NF1, PRG and vimentin show some degree of rescue. RASA2 which does not show a preference for  $G\alpha_{i1}$  vs.  $G\alpha_{i2}$  is not affected by the HD substitution. These data support the idea that the structural differences conferred by the HD of the  $G\alpha_i$  subunits are important for differences in general target engagement beyond PRG.

### **Residue A230 in $G\alpha_{i2}$ controls PRG activation and leads to enhanced proximity interactome engagement**

Since we could not identify individual residues in HD that could confer PRG activation we hypothesized that the HD could be influencing contacts in other regions of  $G\alpha$ . In an existing co-crystal structure of  $G\alpha_{i3}$  bound to the rgRGS domain of PRG<sup>36</sup>, amino acids in the N-terminal portion of the PRG RGS domain bind at the  $G\alpha_{i3}$  HD-RLD domain interface. We hypothesized that this paradigm may extend to PRG interactions with  $G\alpha_{i1}$  as well where the HD may cooperate with the Ras like domain to confer interactions with PRG. Based on this idea we individually substituted non-conserved residues (amino acids conserved between  $G\alpha_{i1}$  and  $G\alpha_{i3}$  but different in  $G\alpha_{i2}$ , starred in Fig. 4A) from the  $G\alpha_{i1}$  RLD into  $G\alpha_{i2}$  and determined if they confer activation of PRG. The majority of the mutations either had no effect or reduced activation, however, substitution of  $G\alpha_{i2}$  A230<sup>S4h3.3</sup> with Asp enables  $G\alpha_{i2}$ (A230D) QL to activate PRG (Fig. 4B, Fig. S2A), while the reverse substitution of D229 to Ala in  $G\alpha_{i1}$  blunts PRG

activation (Fig. 4C). The  $G\alpha_{i2}$  A230D substitution also confers the ability to interact with PRG in a nucleotide-dependent manner in the NanoBiT complementation assay in (Fig. 4D, Fig. S2B). We chose two of the other targets that show differential  $G\alpha_{i1}$  and  $G\alpha_{i2}$  engagement in the proximity labeling western blot assay, NF1 and Parvin, and performed the same assay comparing the QL versions of  $G\alpha_{i1}$ -BioID2,  $G\alpha_{i2}$ -BioID2 and  $G\alpha_{i2}$  A230D-BioID2 (Fig. 4E, Fig. S2C). The A230D substitution enhances the engagement of  $G\alpha_{i2}$  with these other targets. These data support the idea that the structural differences conferred by either the HD, or A230 $G\alpha_{i2}$ /D229 $G\alpha_{i1}$ <sup>s4h3.3</sup>, of the  $G\alpha_i$  subunits are important for differences in general target engagement beyond PRG. Additionally, the observation that these substitutions restore interactions previously identified in a  $G\alpha_{i1}$  BioID proximity labeling screen provides further evidence that these are in fact bona fide  $G\alpha_i$  interaction targets that remain to be further characterized physiologically.

### **$G\alpha_{i1}$ and $G\alpha_{i2}$ sample distinct conformations**

Examination of the static three-dimensional structure of  $G\alpha_{i1}$  does not clearly indicate why substitution at the D229/A230<sup>s4h3.3</sup> position, or substitution of the  $G\alpha_{i1}$  HD, would impact binding and/or activation of target proteins. This amino acid is near the GTP binding site but is not involved in interactions with the nucleotide, and the closest residue in the HD is 9Å away (Fig. 5A and B). To capture potential interactions that may be discerned from the dynamics of these structures, we performed molecular dynamics (MD) simulations with GTP-bound  $G\alpha_{i1}$  and  $G\alpha_{i2}$ . We used the crystal structure of  $G\alpha_i$  (PDB ID:1CIP) as a starting structure for  $G\alpha_{i1}$  and generated a homology model of  $G\alpha_{i2}$  using this structure as a template. MD simulations were run for each system totaling to

5 $\mu$ s. Principal component analysis was used to characterize the dominant motions in  $G\alpha_{i1}$  and  $G\alpha_{i2}$ . Principal Component 1 (PC1) in both proteins is rotation of the HD and RLD relative to one another (Movie S1 and 3). Principal Component 2 (PC2) is a domain “opening” motion where the HD opens relative to the RLD via the interdomain hinge region (Movie S2 and 4). We projected all the snapshots from MD simulations on these two principal components as shown in Fig. 5C. It is evident from Fig. 5C (top panel) that  $G\alpha_{i1}$  and  $G\alpha_{i2}$  sample distinct conformation clusters in these principal component coordinates. MD simulations show that even when bound to GTP, there is some degree of domain opening is possible in both  $G\alpha_{i1}$  and  $G\alpha_{i2}$  but the domain opening is more pronounced in  $G\alpha_{i2}$  compared to  $G\alpha_{i1}$ . When these simulations were done for the mutants  $G\alpha_{i1}$  (D229A) the RLD-HD domain opening moved closer to that of  $G\alpha_{i2}$ . Similarly, with the A230D substitution in  $G\alpha_{i2}$ , moves closer to that of  $G\alpha_{i1}$  in the RLD-HD domain opening coordinate (Fig. 5C bottom panel).

To understand the inter-residue interactions responsible for the differences in domain opening between these G protein subtypes, we analyzed the residues that make the interdomain contacts in the interface in all the MD snapshots. We observed differential interactions between residues in Switch III and the  $\alpha$ D- $\alpha$ E region of the HD in  $G\alpha_{i1}$  compared to  $G\alpha_{i2}$  (Fig. 5D). In  $G\alpha_{i1}$ , two key residues in the HD are involved in an interaction network at the HD-RLD interface, Q147<sup>hdhe.2</sup> and R144<sup>HD.11</sup>. In our simulations during dynamic rotation of the HD-RLD interface, R144<sup>HD.11</sup> dynamically interacts with residues D229<sup>s4h3.3</sup>, D231<sup>s4h3.5</sup>, L232<sup>s4h3.6</sup>, and S228<sup>s4h3.2</sup> in the Switch III region of the RLD, interactions that are not evident in the crystal structure (Fig. 5E left). These interactions are largely absent in  $G\alpha_{i2}$  (Fig. 5E mid). In  $G\alpha_{i2}$ , the cognate residue

for  $G\alpha_{i1}$  D229 is A230, and substitution of A230 with D partially restores many of the interdomain residue interactions with Switch III that are absent in  $G\alpha_{i2}$  relative to  $G\alpha_{i1}$  (Fig. 5E right). Similarly, HD residue Q147<sup>hdhe.2</sup> interacts more frequently with A235<sup>s4h3.9</sup>, R242<sup>H3.1</sup>, and V233<sup>s4h3.7</sup> in  $G\alpha_{i1}$  than the cognate interactions in  $G\alpha_{i2}$ . When  $G\alpha_{i2}$  A230<sup>s4h3.3</sup> is substituted with D interactions between Q148<sup>hdhe.2</sup> and V234<sup>s4h3.7</sup> are strengthened, with other contacts are largely unaffected. This supports the idea that  $G\alpha_{i1}$  D229 stabilizes a network of interactions between the HD and RLD-Switch III that are lost in  $G\alpha_{i2}$  (Fig. 5D).

### **Bayesian network models show that $G\alpha_{i2}$ A230D mimics $G\alpha_{i1}$ in RLD-HD interactions**

As another approach, a fingerprint matrix of Switch III-HD residue contacts was constructed using data from the simulations. Bayesian Network Analysis was performed on this matrix, yielding a full Bayesian network (shown in Fig. S3 of Supporting Information) for these contacts in  $G\alpha_{i1}$  and  $G\alpha_{i2}$  and their mutants. Each node in this network model represents a residue interaction pair between RLD and HD. Nodes were then ranked by strength to understand their cooperativity ranking within the network. This analysis shows that interactions between D229<sup>s4h3.3</sup> in the RLD and R144<sup>HD.11</sup> in the HD forms the core of a cooperativity network involving multiple contacts in Switch III (Fig. 5F, left panel). This interaction network is disrupted in  $G\alpha_{i2}$  where the D229 cognate residue is alanine ( $G\alpha_{i2}$  A230) which cannot interact with the positively charged arginine ( $G\alpha_{i2}$  R145<sup>HD.11</sup>) (Fig. 5F, center panel). Substitution of A230 with D in  $G\alpha_{i2}$  restores a cooperative interaction network with Switch III (Fig.5F, right panel). This analysis supports the idea that in GTP-bound  $G\alpha_{i1}$ , D229 at the base of Switch III forms

an important contact with R144 in the HD that is not observed in crystal structures of  $G\alpha_{i1}$ . This interaction supports a network of additional interactions between the HD and multiple amino acids in Switch III that constrain the conformation of Switch III. This network does not form in  $G\alpha_{i2}$ , likely permitting Switch III to adopt conformations other than that seen in  $G\alpha_{i1}$ , leading to lower-efficacy interactions with effectors that require Switch III for activation.

### **PRG stimulation is dependent on interdomain stabilization of $G\alpha_i$ Switch III**

The simulation data indicate that an ionic interaction between D229 in the RLD and R144 in the HD centers an interaction network that controls the conformation of Switch III. Based on this we predicted that mutation of R144 to disrupt this interaction would reduce PRG activation by  $G\alpha_{i1}$ .  $G\alpha_{i1}$  R144A reduces nucleotide-dependent PRG activation in cells, similar to that of  $G\alpha_{i1}$  D229A. When alanine is substituted for both D229 and R144, the same reduction is observed (Fig. 6A). Alanine substitution of cognate residue R145 in  $G\alpha_{i2}$  does not alter nucleotide-dependent PRG activation, but completely abolishes activation of PRG conferred by A230D (Fig. 6B). These experiments show that the D229-R144 interaction contributes to the ability of  $G\alpha_{i1}$  to activate PRG, and the ability to activate PRG conferred to  $G\alpha_{i2}$  by the A230D substitution is entirely dependent on the interdomain D230-R145 interaction.

In the Ras-like domain are the switch regions including the Switch III loop. Switch III is critical for communication to the HD across the domain interface, and affects multiple aspects of  $G\alpha$  protein function, including effector recognition<sup>37,38</sup> and receptor-

mediated activation<sup>39</sup>. In the cocrystal structure of  $G\alpha_{13}$  and PRG, Switch III makes multiple contacts with PRG. To test involvement of Switch III in  $G\alpha_i$ -dependent PRG activation, we substituted  $G\alpha_{i1}$  Switch III residues D231 – A235 (DLVLA) to cognate  $G\alpha_s$  residues N254 – R258 (NMVIR) ( $G\alpha_{i1}$  SW3 $\alpha$ S).  $G\alpha_{i1}$  SW3 $\alpha$ S QL poorly activated PRG compared to  $G\alpha_{i1}$  QL in the SRE luciferase assay (Figs. 7A and B). The loss-of-function mutations in Switch III along with the gain-of-function phenotype achieved by substitution of either  $G\alpha_{i1}$  RLD elements or HD elements provide evidence of cooperation between the RLD and HD stabilizing Switch III in a conformation needed for  $G\alpha_i$ -mediated activation of PRG, and likely other targets, that is lost in  $G\alpha_{i2}$ .



## **Discussion**

In this study, we provide evidence that  $G\alpha_i$ -effector interactions are dependent on the strength and frequency of interaction between Switch III residues and the HD in the GTP bound state, and that these interactions differ between  $G\alpha_i$  subtypes. The data show that  $G\alpha_{i2}$  has fewer interdomain residue contacts, leading to weaker interactions between Switch III in the RLD and HD. Interruption of these contacts limits the ability of  $G\alpha_i$  to activate PRG. It is likely that stabilization of Switch III is central to this mechanism because Switch III conformational changes are dependent on the nucleotide binding state (GTP vs. GDP) while the conformation of the HD is generally not altered upon GTP binding. While we focused on PRG stimulation as a functional indicator of  $G\alpha_i$  specificity, the  $G\alpha_i$ -BioID proximity labeling experiments demonstrate that there are global differences in GTP-dependent interactions between  $G\alpha_i$  subtypes and several novel targets, and that these differences depend on the same substitutions of residues from  $G\alpha_{i1}$  into  $G\alpha_{i2}$  that conferred specificity for PRG activation. This result indicates stabilization of interdomain interactions in the GTP state may play an unappreciated role

in the downstream signaling function of  $G\alpha_i$  subunits, and a major role in differentiating  $G\alpha_i$  subtype function.

The involvement of the  $G\alpha_{i1}$  D229-R144 interaction and other additional interdomain contacts in stabilization of Switch III and effector interactions are supported by multiple key results. First, computational simulations show a dynamic interaction landscape where single substitutions affect the strength of other regional contacts. Second, substitution of either the  $G\alpha_{i1}$  HD or A230D into  $G\alpha_{i2}$  results in increased, GTP-dependent interaction with PRG and other protein targets compared to  $G\alpha_{i2}$  QL. Third, the effects of A230D in the RLD are completely abrogated if R145 in the HD is changed to alanine, strongly supporting the idea that this interdomain linkage is key to stabilizing the interface and Switch III such that it can interact with targets.

Position s4h3.3 ( $G\alpha_{i1}$  D229 and  $G\alpha_{i2}$  A230) is unique for the  $G\alpha_i$  subfamily in that the residue is different for each  $G\alpha$  family but is conserved within each family except  $G\alpha_i$ . Amino acids at this position for each family include Ser in  $G\alpha_s$ , Gly in  $G\alpha_o$  and  $G\alpha_z$ , Ala in  $G\alpha_T$ , and Glu in  $G\alpha_{q/11}$  and  $G\alpha_{12/13}$  (Fig. S5). A similar ionic lock mechanism for stabilization of Switch III through interdomain interactions is likely conserved in the  $G\alpha_{q/11}$  family and also  $G\alpha_{13}$ , as  $G\alpha_{i1}$  R144<sup>HD.11</sup> is conserved in these G proteins and could interact in a similar way with Glu at s4h3.3 in Switch III. Despite the similarities to other  $G\alpha$  subunits at these positions, the  $G\alpha_i$  subfamily seems unique in its intra-family effector specificity achieved by differentiation at s4h3.3 resulting in the presence or absence of the ionic lock.

RLD-HD interactions have classically been understood to be a regulator of nucleotide exchange <sup>12,40-45</sup>, with mutations at the interface intended to disrupt interactions leading to higher rates of GDP dissociation <sup>12</sup>. Specifically, mutation of residue R144 in  $G\alpha_{i1}$  to an alanine is known to significantly increase the rate of GTP $\gamma$ S binding, presumably through the breaking of an interdomain interaction with L232 <sup>12</sup>. In  $G\alpha_s$ , substitution of residues in the Switch III loop to those of  $G\alpha_{i2}$  disrupt the ability of  $G\alpha_s$  to bind GTP in response receptor activation, but retains the ability to activate AC in response to GTP $\gamma$ S activation. Activation can then be restored by additionally substituting the  $G\alpha_s$  HD with  $G\alpha_{i2}$  residues <sup>39,46</sup>, demonstrating the importance of G $\alpha$  isoform-specific interdomain communication for receptor dependent G protein activation.

Co-crystal structures of G $\alpha$  subunits in each family have shown all non-RGS effectors binding to a common cleft between the  $\alpha 2$  (Switch II) and  $\alpha 3$  helices with no apparent direct involvement of Switch III <sup>36,47-51</sup>. On the other hand, mutagenic analysis  $G\alpha_q$ -GRK2 interactions revealed involvement of both the HD and Switch III <sup>52</sup>, an interaction not evident in the co-crystal structure of  $G\alpha_q$  with GRK2. As another example,  $G\alpha_{T1}$  binding to the autoinhibitory  $\gamma$  subunit of cGMP phosphodiesterase (PDE $\gamma$ ) is dependent on the presence of the HD <sup>53</sup>, however the binding site of PDE $\gamma$  is not in the HD but rather in the  $\alpha 2$ - $\alpha 3$  cleft <sup>51</sup>. Crucially, mutation of a Switch III Glu to Leu abolishes PDE activation by  $G\alpha_T$ , with no effects on nucleotide binding or hydrolysis <sup>37</sup>. A recent cryo-EM structure of the full cGMP PDE6  $\alpha\beta\gamma$  complex with transducin revealed the binding of PDE $\gamma$  to the outer edge of the Switch III loop as well as the previously solved site in the  $\alpha 2$ - $\alpha 3$  cleft in  $G\alpha_T$ -GTP <sup>54</sup>. Thus, there is evidence for

involvement of Switch III in effector engagement and our analysis reveals how two proteins with identical Switch III residues can have differences in target engagement efficacy.

While it remains untested how the lower efficacy of target engagement by  $G\alpha_{i2}$  relative to  $G\alpha_{i1}$  directly leads to distinct physiological roles, our findings are consistent with the notion that  $G\alpha_{i2}$  may in some situations act primarily to regulate AC and act as a scaffold and switch for  $G\beta\gamma$  signaling, whereas  $G\alpha_{i1}$  or  $G\alpha_{i3}$  may perform these functions in addition to signaling to various  $G\alpha_i$ -specific effectors. This is consistent with known roles for  $G\alpha_{i2}$  and  $G\alpha_{i3}$ -mediated signaling events in neutrophils, where  $G\alpha_{i2}$  activation promotes cell arrest while and  $G\alpha_{i3}$  promotes migratory phenotypes <sup>27</sup>. Eosinophils from  $G\alpha_{i2}$  whole-body knockout mice display enhanced chemotactic responses *in vitro* <sup>55</sup>. The effects of activation of  $G\alpha_{i2}$  on neutrophil arrest in cells lacking  $G\alpha_{i3}$  are similar to those found by  $G\beta\gamma$  activation alone <sup>56</sup>. The physiological situation is likely to be more complex and this model cannot fully explain physiological specificity. For example, in murine atria, GIRK channel activity is differentially regulated by  $G\alpha_{i2}$  and  $G\alpha_{i1}/G\alpha_{i3}$ . Deletion of  $G\alpha_{i2}$  increases  $G\beta\gamma$ -mediated basal and agonist-induced GIRK currents, while dual knockout of  $G\alpha_{i1}$  and  $G\alpha_{i3}$ , which are known to bind and regulate GIRK, ablates basal and muscarinic agonist-induced GIRK activity <sup>57</sup>. Nevertheless, it is probable that regulation of interdomain dynamics through the intramolecular interactions we defined play a significant role in physiological specificity.

In conclusion, we describe here a previously unknown mechanism of effector specificity between  $G\alpha_i$  subtypes. Switch III is stabilized by an interdomain interaction

network with  $\alpha$ D- $\alpha$ E residues in the helical domain, due in part to rearrangement of one non-conserved  $G\alpha_i$  Switch III aspartate that contacts a conserved arginine. This stabilization of Switch III not only confers specificity for activation of  $G\alpha_{i1/3}$  effector PDZ-RhoGEF, but for interaction with an array of additional protein targets, shedding light on a fundamental mystery of functional redundancy among this highly similar  $G\alpha$  protein family.

## **Methods**

### **Plasmid cDNA constructs**

BioID2 fused N-terminally with c-Myc tag and C-terminally with mVenus, followed by CaaX PM targeting motif (KKKKKSKTKCVIM, derived from the C terminus of KRas), was a gift from S. Malik of the University of Rochester. C-terminally c-Myc-tagged full-length PRG cDNA construct in mammalian expression vector was a gift from J. Tesmer of Purdue University. The following plasmids were obtained from Addgene: mEmerald-parvin-C-14 (#54214), EGFP-vimentin-7 (#56439), HA-G $\alpha_i$ -BioID2 plasmids in pcDNA3.1+ were constructed as described previously<sup>29</sup>.

All G $\alpha$  clones in pcDNA3.1+ were obtained from the cDNA Resource Center. The sequences of the clones are available upon request.

All mutagenesis to G $\alpha_i$  DNA constructs was accomplished using reagents, protocols, and guidelines from New England Biolabs Q5® Site-Directed Mutagenesis Kit (E0554S). G $\alpha_{i2}$ -1HD, all G $\alpha_{i1}$  HD subdivision constructs, and G $\alpha_i$  N- and C-terminal substitutions were generated using reagents, protocols, and guidelines from New England Biolabs HiFi DNA Assembly Master Mix (E2621) and Cloning Kit (E5520).

In G $\alpha_{i1}$ , a FLAG epitope (DYKDDDDK) was inserted between Ala 121 and Glu 122 and flanked by a flexible linker (SGGGGS) on both sides of the insert. The FLAG epitope in G $\alpha_{i2}$  was inserted in the same manner with the same linkers at the analogous position as G $\alpha_{i1}$ , between Asp 122 and Asp 123.

G $\alpha_{i1}$  SW3 $\alpha$ S-FLAG was generated using Q5 mutagenesis by substituting G $\alpha_s$  residues N254 – R258 (NMVIR) into their cognate position in G $\alpha_{i1}$ , D231 – A235 (DLVLA) in FLAG-tagged G $\alpha_{i1}$ .

SmBiT-PRG was generated by inserting the SmBiT sequence (VTGYRLFEEIL) followed by a flexible linker (SGGGGS) onto the N-terminus of cMyc-PRG (cMyc: EQKLISEEDL), resulting in SmBiT-Linker-cMyc-PRG.

### **Cell Culture**

A293 and HT1080 cells were obtained from the American Type Culture Collection. A293 and HT1080 cells were grown supplemented in DMEM (Dulbecco's modified Eagle medium) with 10% fetal bovine serum (FBS) (10437028, Gibco) and 100 U of penicillin/streptomycin (15140122, Gibco) at 37°C with 5% CO<sub>2</sub>. Trypsin-EDTA (25200056, Gibco) was used for cell passage.

### **Reagents**

The following primary and secondary antibodies were used: G $\alpha_{i1/2}$  (anti-sera)<sup>58</sup>, c-Myc (13-2500, Invitrogen), GFP (A11122, Invitrogen), HA (C29F4, Cell Signaling), FLAG

(PA1-984B, Invitrogen). Streptavidin-IRDye800 was from LI-COR (925-32230). Primary antibodies were diluted in 3% bovine serum albumin (BSA) and 0.1% sodium azide and incubated with blots overnight at 4°C. Streptavidin-IRDye800 was incubated for 1 hour at room temperature. For secondary antibodies, goat anti-rabbit DyLight 800 (SA535571, Invitrogen) and goat anti-mouse IRDye 800CW (926-32210, LI-COR) were used at 1:10,000.

### **NanoBiT Luciferase Complementation Assay**

$6.0 \times 10^5$  HEK293A cells were seeded in poly-D-lysine coated 6-well plates (Fisher FB012927). Immediately after plating, HA-G $\alpha$ -LgBiT constructs and SmB-cmyc-PDZ-RhoGEF were co-transfected using a 1:3 mass to volume ratio of DNA to Lipofectamine 2000 (Invitrogen). After 24 hours, transfection media was aspirated and cells were gently washed once with 1 mL warm PBS. The PBS was discarded, 200  $\mu$ L trypsin solution was added, and the plate was incubated at 37°C and 5% CO<sub>2</sub> for 5 mins. Following incubation, 800  $\mu$ L of warm 1X HBSS was added to each well, and the detached cells were aspirated and dispensed into new 15 mL conical tubes. Cells were then pelleted by centrifugation at 250 x g for 5 mins at RT. After carefully aspirating the supernatant, each pellet was resuspended in 1 mL warm HBSS, and cell number in each suspension counted. Cell suspensions were centrifuged once more at 250 x g for 5 mins at RT and resuspended in warm 10  $\mu$ M furimazine in HBSS, 1% DMSO.  $5 \times 10^4$  cells were distributed to each well in a 96-well plate; samples were analyzed with six technical replicates. The sample plate was incubated at 37°C for 15 mins, followed by a luminescence measurement in each well.

### **SRE-Luciferase Reporter Assay**

#### *96-well format*

$4.5 \times 10^4$  HEK293A cells were seeded in poly-D-lysine coated 96-well plates (Greiner 655983). Cells were transfected with the following plasmids and amounts per well: 25 ng SRE-Luc reporter (E134A, Promega), 75 ng G $\alpha_i$  or G $\alpha_i$  QL in pcDNA3.1+, 2.5 ng cmyc-PRG unless otherwise indicated. Minor adjustments in added DNA were made to equalize expression of G $\alpha_i$  subunits based on western blotting of Flag tagged constructs. In these cases, empty pcDNA3.1+ vector supplemented to equalize total DNA added per well. Transfection took place immediately after seeding with a 1:3 mass to volume ratio of DNA to Lipofectamine 2000 (Invitrogen). Twelve hours after transfection, the media was replaced with 75  $\mu$ L of serum-free media. Twenty-four hours after transfection, 75  $\mu$ L (1:1 volume) of One-Glo reagent (E6110, Promega) was added to each well and incubated for 10 min at room temperature. The luminescence signal was measured using Varioskan LUX multimode microplate reader (Thermo Fisher Scientific).

### *24-well format*

The SRE-Luc reporter assay was also performed nearly identically in 24-well plates, which offered better well-to-well consistency for technical replicates.  $1 \times 10^5$  HEK293A cells were seeded in poly-D-lysine coated 24-well plates. One hundred ng SRE-Luc reporter (E134A, Promega), 300 ng  $G\alpha_i$  or  $G\alpha_i$  QL in pcDNA3.1+, and 5 ng myc-PRG DNA were transfected into each well except in  $G\alpha_i$  titration experiments, where reduced  $G\alpha_i$  DNA was substituted with empty pcDNA3.1+. Transfection took place immediately after seeding with a 1:3 mass to volume ratio of DNA to Lipofectamine 2000 (Invitrogen). Twelve hours after transfection, the media was replaced with 250  $\mu$ L of serum-free media. Twenty-four hours after transfection, 250  $\mu$ L (1:1 volume) of One-Glo reagent (E6110, Promega) was added to each well and incubated for 10 min at room temperature. The luminescence signal was measured using Varioskan LUX multimode microplate reader (Thermo Fisher Scientific). We found that the fold differences in activation by  $G\alpha_i$  were lower in the 24 well format but that the technical replicates were more reliable.

### **GloSensor cAMP Assay**

$4.5 \times 10^4$  HEK293A cells were seeded in poly-D-lysine coated 96-well plates (Greiner 655983). Cells were transfected with the following plasmids and amounts per well: 50 ng GloSensor -20F cAMP plasmid (E1171, Promega), 125 ng  $G\alpha_i$  or  $G\alpha_i$  QL in pcDNA3.1+. In  $G\alpha_i$  titration experiments, DNA was supplemented with empty pcDNA3.1+ vector. Transfection took place immediately after seeding with a 1:3 mass to volume ratio of DNA to Lipofectamine 2000 (Invitrogen). Twenty four hours post-transfection, the media was discarded and the cells were loaded with 75  $\mu$ L 0.5 mg/mL D-Luciferin (L2916, Sigma Aldrich) in Leibowitz's L-15, incubating for 2 hours at 37°C and 5% CO<sub>2</sub>.

### **Western blotting**

Samples in 1X Laemmli sample buffer were resolved on 4-20% gradient Mini-PROTEAN TGX gels (4561094, Bio-Rad), transferred to nitrocellulose membranes (Pall 66485), and stained with Ponceau S (141194, Sigma Aldrich). Membranes were blocked with 3% bovine serum albumin (141194, Sigma Aldrich) in TBST (0.1% Tween-20 in 20 mM Tris pH 7.5 + 150 mM NaCl) at room temperature (RT) for 30 min with constant agitation. Primary antibodies were applied for 2 hours at RT or overnight at 4°C. After three RT washes with TBST at 5 min each, secondary antibodies were applied for 1 hour. Membranes were imaged on an Odyssey Infrared Imaging System (LI-COR Biosciences).

### **Bioid2 proximity labeling and tandem mass spectrometry analysis**

HT1080 cells at passage number up to 15 were used for proximity labeling experiments. Cells were plated into 175 cm<sup>2</sup> flasks at a density of  $5.5 \times 10^6$  cells per flask. The next



day, media was replaced with 35 mL of DMEM containing 50  $\mu$ M biotin and 10% FBS. Each flask was transfected with 8  $\mu$ g of plasmid encoding Biold2-fused  $G\alpha_i$  construct and 4  $\mu$ g of YFP cDNA. A total of 0.6  $\mu$ L of Viomer Red (VR-01LB-00, Lipocalyx, Germany) reagent was used per 2  $\mu$ g of cDNA for transfection, resulting in ~80 to 85% transfection efficiency. Twenty-four hours after labeling and transfection, the labeling medium was decanted, cells were washed twice with 1 $\times$  PBS, and harvested at 4000  $\times$  g for 10 min. This step was repeated twice using 1 $\times$  PBS to recover the maximum number of cells. The supernatant was aspirated, and pellets were flash-frozen and stored at  $-80^{\circ}\text{C}$  until further use.

All stock solutions used for streptavidin pulldown were freshly prepared, except lysis buffer. Low protein binding tubes (022431081, Eppendorf) were used for sample preparation. Frozen pellets were lysed in 1 mL of ice-cold lysis solution (composition described above) for 10 min on ice and incubated with 125 U of benzonase with end-over-end rotation at  $4^{\circ}\text{C}$  for 20 min. A total of 0.3% SDS was added to lysates, which were incubated for another 10 min at  $4^{\circ}\text{C}$ . Lysates were centrifuged at 15,000  $\times$  g for 15 min. The supernatant was transferred to fresh tubes, and the total protein concentration was measured using Pierce 660 nm protein assay reagent. A total of 5% of lysates, adjusted for protein concentration, was reserved to analyze the biotinylation in inputs. The remaining lysates were incubated with 500  $\mu$ L of Pierce streptavidin magnetic beads slurry per sample in an end-over-end rotator at  $4^{\circ}\text{C}$  overnight. Beads were washed twice with modRIPA buffer [modRIPA: 50 mM tris, 150 mM NaCl, 0.1% SDS, 0.5% sodium deoxycholate, and 1% Triton X-100 (final pH 7.5)] and once with four different solutions: 1 M KCl, 0.1 M  $\text{Na}_2\text{CO}_3$ , 2% SDS [in 50 mM tris (pH 7.5)], and 2 M urea [in 10 mM tris (pH 8.0)]. Beads were washed twice with 1 $\times$  PBS and were flash-frozen and stored at  $-80^{\circ}\text{C}$  until further processed for MS.

### **Biold2 proximity labeling and immunoblot analysis**

$1.5 \times 10^6$  HEK293A cells were seeded in a poly-D-lysine coated 10 cm plate. The next day, media was replaced with 10 mL DMEM +10% FBS and biotin was added to 50  $\mu$ M. Cells were transfected with 3  $\mu$ g of either Biold-CAAX or one of the  $G\alpha_i$ -Biold2-HA constructs in pcDNA3.1+, in addition to 3  $\mu$ g of one of the effectors of interest (myc-PRG, V5-ADNP, RASA2-FLAG, mEmerald-Parvin, RSK1-HA, or GFP-Vimentin). DNA complexes were added to Lipofectamine 2000 solutions with a 1:3 mass:volume ratio (18  $\mu$ L per plate). After 24 hours of expression and labeling, the medium was decanted, cells were rinsed twice with 5 mL of ice cold 1X PBS, scraped off of the plate, and pelleted at  $4^{\circ}\text{C}$  and 4000  $\times$  g for 10 min. The supernatant was aspirated and the cell pellets were flash-frozen with liquid  $\text{N}_2$  and stored at  $-80^{\circ}\text{C}$  until processed via IP.

For the IP, 500  $\mu$ L ice cold modRIPA was used to resuspend cell pellets. Lysis using benzonase and SDS proceeded as above. Lysates were centrifuged for 15,000  $\times$  g for 15 min at  $4^{\circ}\text{C}$ , and protein concentration was measured using Pierce 660 nm protein assay reagent. After equalizing for protein concentration, 20  $\mu$ L of each sample volume was retained as an input sample. Five hundred  $\mu$ L of each equalized sample was added to 170  $\mu$ L of Pierce streptavidin magnetic bead slurry and rotated end-over-end at  $4^{\circ}\text{C}$

for at least 2 hours to capture biotinylated proteins. Beads were washed three times with ice cold modRIPA and once more with cold 1X PBS. Beads were then resuspended in 100  $\mu$ L 1X PBS, and 4X Laemmli sample buffer was added to 1X final concentration. Beads were boiled for 10 min at 95°C, and the supernatant was analyzed by western blot using anti-HA (1:2000) for G $\alpha$ <sub>i</sub>-BioID2-HA and the corresponding antibody for each protein of interest [cmyc-PRG – anti-cmyc (1:2000), V5-ADNP – anti-V5 (1:1000), RASA2-FLAG – anti-FLAG (1:1000), mEmerald-Parvin – anti-GFP (1:1000), RSK1-HA – anti-HA (1:2000), or GFP-Vimentin – anti-GFP (1:1000)].

## Protein digestion and TMT labeling

On-bead digestion followed by liquid chromatography–tandem MS (LC-MS/MS) analysis was performed at the MS-based Proteomics Resource Facility of the Department of Pathology at the University of Michigan. Samples were reduced (10 mM dithiothreitol in 0.1 M triethylammonium bicarbonate (TEAB) at 45°C for 30 min), alkylated (55 mM 2-chloroacetamide at room temperature for 30 min in the dark), and subsequently digested using a 1:25 ratio of trypsin (V5113, Promega):protein at 37°C with constant mixing. A total of 0.2% trifluoroacetic acid was added to stop the proteolysis, and peptides were desalted using a Sep-Pak C18 cartridge (WAT036945, Waters Corp). The desalted peptides were dried in a vacufuge and reconstituted in 100  $\mu$ L of 0.1 M TEAB. A TMT10plex Isobaric Label Reagent Set plus TMT11-131C Label Reagent kit (A37725, Thermo Fisher Scientific) was used to label each sample per the manufacturer's protocol. The samples were labeled with TMT 11-plex reagents at room temperature for 1 hour. The reaction was quenched by adding 8  $\mu$ L of 5% hydroxylamine for 15 min and dried. An offline fractionation of the combined sample into eight fractions was performed using a high pH reverse-phase peptide fractionation kit, as per the manufacturer's protocol (84868, Pierce). Fractions were dried and reconstituted in 12  $\mu$ L of 0.1% formic acid/2% acetonitrile for LC-MS/MS analysis.

## LC-MS analysis

An Orbitrap Fusion (Thermo Fisher Scientific) and RSLC Ultimate 3000 nano-UPLC (Dionex) were used to acquire the data. For superior quantitation accuracy, we used multinotch-MS3<sup>59</sup>. Two microliters of each fraction was resolved on a nanocapillary reverse-phase column (75  $\mu$ m internal diameter by 50 cm; PepMap RSLC C18 column, Thermo Fisher Scientific) at a flowrate of 300 nL/min using 0.1% formic acid/acetonitrile gradient system (2 to 22% acetonitrile in 110 min; 22 to 40% acetonitrile in 25 min; 6-min wash at 90% acetonitrile; 25 min re-equilibration) and directly sprayed onto the Orbitrap Fusion using EasySpray source (Thermo Fisher Scientific). The mass spectrometer was set to collect one MS1 scan [Orbitrap; 120,000 resolution; AGC target  $2 \times 10^5$ ; max IT (maximum ionization time) 50 ms] and data-dependent, "Top Speed" (3 s) MS2 scans [collision-induced dissociation; ion trap; NCE (normalized collision energy) 35; AGC (automatic gain control)  $5 \times 10^3$ ; max IT 100 ms]. For multinotch-MS3, the top 10 precursors from each MS2 were fragmented by high energy collisional dissociation (HCD), followed by Orbitrap analysis (NCE 55; 60,000 resolution; AGC  $5 \times 10^4$ ; max IT 120 ms, 100 to 500 mass/charge ratio scan range).

## Generating structural models and molecular dynamics simulations

The structural model of monomeric GTP-bound  $G\alpha_{i1}$  and  $G\alpha_{i2}$  protein with  $Mg^{2+}$  ion was built using the monomeric GTP bound rat  $G\alpha_{i1}$  crystal structure (PDB ID: 1CIP) as template and using the homology modeling method in the Prime module of Maestro software from Schrodinger (<https://www.schrodinger.com/products/maestro>). The GNP present in the original crystal structure was converted to GTP using Maestro edit panel. Point mutations to generate the structures of  $G\alpha_{i1}^{D229A}$  and  $G\alpha_{i2}^{A230D}$  were performed using Maestro Biologics suite. The side chain packing was done for all the residues within 5Å of the mutated residue position including the mutated residues using Maestro Prime suite. All structures further underwent energy minimization using conjugate gradient method with a convergence cutoff of 0.1kcal/mol/Å. Input files for molecular dynamics simulations were generated using CHARMM-GUI<sup>60</sup>. Each monomeric  $G\alpha_i$  protein was solvated in explicit TIP3P water molecules in a cubic box (9.0nm x 9.0nm x 9.0nm) with 0.15M of potassium chloride to mimic the physiological condition. We used GROMACS software<sup>61</sup> (Version 2021.3) with all-atom CHARMM36 force field<sup>62</sup> to perform molecular dynamics simulations. MD simulations were performed at 310°K coupled to a temperature bath with a relaxation time of 0.1ps<sup>63</sup>. Pressure of the systems was calculated with molecular virial and was held constant by a weak coupling to a pressure bath with a relaxation time of 0.5ps. Equilibrium bond length and geometry of water molecules were constrained using the SHAKE algorithm<sup>64</sup>. The short-range electrostatic and van der Waals interactions were estimated every 2fs using a charged group pair list with cutoff of 8Å between centers of geometry of charged groups. Long-range van der Waals interactions were calculated using a cutoff of 14Å and long-range electrostatic interactions were treated with the particle mesh Ewald method<sup>65</sup>. Temperature was kept constant at 310°K by applying the Nose-Hoover thermostat<sup>66</sup>. Desired pressure for all systems were achieved by using Parrinello-Rahman barostat with a pressure relaxation time of 2ps<sup>67</sup>. Before production runs, all system were subjected to a 5000-step steepest descent energy minimization to remove bad contacts<sup>68</sup>. After minimization, the systems were heated up to 310°K under constant temperature-volume ensemble (NVT). The simulations were saved every 200ps for analysis. The protein,  $Mg^{2+}$  ion, and nucleotide were subjected to positional constraints under a harmonic force constant of 1000 kJ/(mol\*nm<sup>2</sup>) during the NVT step while solvent molecules were free to move. The systems then were further equilibrated using a constant pressure ensemble (NPT), in which the force constant is applied to the protein,  $Mg^{2+}$  ion, and nucleotide were gradually reduced from 5kJ/(mol\*nm<sup>2</sup>) to zero in six steps of 5ns each. An additional 50ns of unconstraint simulation was performed, making it a total of 80ns NPT equilibration prior to production runs. We performed five production runs of 1000ns each using five different initial velocities for every system. Therefore, we had 5µs long MD trajectories for both WT and mutant systems of  $G\alpha_{i1}$  and  $G\alpha_{i2}$  protein.

## Principal Component Analysis and representative structures

The last 600ns of five independent molecular dynamics simulation runs were merged into one concatenated trajectory for each system. Two merged trajectories were further created based on the concatenated trajectories: one contains the WT  $G\alpha_{i1}$  and  $G\alpha_{i2}$  trajectories, and the other contains all four trajectories. Principal component analysis was performed on each merged trajectory using the gmx covar module of GROMACS with covariance matrix of C alpha atoms of all residues. The first two principal components (PC1 and PC2) of every system were extracted using gmx ana eig module of GROMACS and imported into Python as a data-frame using the Pandas package. Kernel density estimation maps were generated using Python Seaborn package (version 0.9.0) and plotted using Python Matplotlib package.

### Representative structure extraction

Using Get-contact data (see previous), frame numbers in  $G\alpha_{i2}^{A230D}$  trajectory that have contacts between R145 and D230 were recorded. The corresponding frames were extracted from the trajectory using gmx trjconv module of GROMACS. The representative structure of  $G\alpha_{i1}$  was used as template, and the root-mean-square deviation (RMSD) values of the extracted  $G\alpha_{i2}^{A230D}$  frames were calculated using gmx rms module: C alpha atoms were selected for both alignment and calculation. The frame with the smallest RMSD value was selected as the representative structure for  $G\alpha_{i2}^{A230D}$  system.

### Calculating the fingerprints of pairwise interactions between AHD and switch III domain of G protein

The analysis of the landscape of pairwise intermolecular residue contacts between AHD domain and switch III region of  $G\alpha_i$  with MD simulations using the "getcontacts" python script library (<https://www.github.com/getcontacts>). This was utilized to identify various types of contacts, including salt-bridges (<4.0 Å cutoff between anion and cation atoms), hydrogen bonds (<3.5 Å cutoff between hydrogen donor and acceptor atoms, <70° angle between donor and acceptor), van der Waals (<2 Å difference between two atoms), pi-stack contacts (<7.0 Å distance between aromatic centers of aromatic residues, <30° angle between normal vectors emanating from aromatic plane of each residue), and cation-pi contacts (<6.0 Å distance between cation atom and centroid of aromatic ring, <60° angle between normal vector from aromatic plane to cation atom). To conduct the analysis, the MD simulation trajectories were concatenated into 1μs ensembles and stored as xtc coordinate files. Subsequently, water and ions were stripped from the trajectory files utilized for the contact analysis, and atom selection groups were matched with the relevant amino acid residues for each protein domain. In-house python scripts were used to perform one-hot encoding to generate a binary fingerprint for each simulation. The one-hot encoding represented the presence of a contact between two residues in a particular frame with "1" and its absence with "0".

### Bayesian Network Analysis

Binary fingerprints of residue contact pairs were analyzed to understand their interdependent interactions using BNOmics, software developed for Bayesian network analysis. Separate BNs were first constructed for each G protein type. Heuristic network model selection search<sup>69</sup> was carried out with 50 random restarts, to ensure convergence. Bayesian networks of contact fingerprints have residue pairs as nodes and the edge weight between the nodes correlates with the dependency between them. As a measure of contact pairs' connectivity, the network property of node strength was used - the total sum of edge weights belonging to this node. After sorting the residue pairs from highest node strength to the lowest, the top 25 percentile of them was compared between different G protein types. Graphical representation of these nodes and their interconnections were demonstrated using network visualization software Cytoscape 3.9.1 (<https://cytoscape.org/>).

### **Supplemental Movies**

Movie S1. Video of PC1 movements in GTP-bound G $\alpha_{i1}$

Movie S2. Video of PC2 movements in GTP-bound G $\alpha_{i1}$

Movie S3. Video of PC1 movements in GTP-bound G $\alpha_{i2}$

Movie S4. Video of PC2 movements in GTP-bound G $\alpha_{i2}$

### **Author Contributions**

TJL performed experiments, participated in experimental design, wrote the manuscript. WW performed experiments, participated in experimental design, and edited the manuscript. EM performed experiments, participated in experimental design, and edited the manuscript. SMV performed experiments. NC participated in experimental design. SA performed experiments, NV participated in experimental design and edited the manuscript, AVS participated in experimental design and edited the manuscript.

### **Research Funding**

AVS NIH R35GM127303, TJL AHA 826816, NV R01-GM117923 and R01-LM013876

## References

1. Sriram, K. & Insel, P.A. G Protein-Coupled Receptors as Targets for Approved Drugs: How Many Targets and How Many Drugs? *Mol Pharmacol* **93**, 251-258 (2018).
2. Hauser, A.S., Attwood, M.M., Rask-Andersen, M., Schioth, H.B. & Gloriam, D.E. Trends in GPCR drug discovery: new agents, targets and indications. *Nat Rev Drug Discov* **16**, 829-842 (2017).
3. Gilman, A.G. G proteins: transducers of receptor-generated signals. *Annu Rev Biochem* **56**, 615-49 (1987).
4. Hepler, J.R. & Gilman, A.G. G proteins. *Trends Biochem Sci* **17**, 383-7 (1992).
5. Oldham, W.M. & Hamm, H.E. Heterotrimeric G protein activation by G-protein-coupled receptors. *Nat Rev Mol Cell Biol* **9**, 60-71 (2008).
6. Calebiro, D., Koszegi, Z., Lanoiselee, Y., Miljus, T. & O'Brien, S. G protein-coupled receptor-G protein interactions: a single-molecule perspective. *Physiol Rev* **101**, 857-906 (2021).
7. Coleman, D.E. et al. Structures of active conformations of Gi alpha 1 and the mechanism of GTP hydrolysis. *Science* **265**, 1405-12 (1994).
8. Knight, K.M. et al. A universal allosteric mechanism for G protein activation. *Mol Cell* **81**, 1384-1396 e6 (2021).
9. Van Eps, N. et al. Interaction of a G protein with an activated receptor opens the interdomain interface in the alpha subunit. *Proceedings of the National Academy of Sciences* **108**, 9420-9424 (2011).
10. Chung, K.Y. et al. Conformational changes in the G protein Gs induced by the  $\beta$ 2 adrenergic receptor. *Nature* **477**, 611-615 (2011).
11. Rasmussen, S.G.F. et al. Crystal structure of the  $\beta$ 2 adrenergic receptor-Gs protein complex. *Nature* **477**, 549-555 (2011).
12. Remmers, A.E., Engel, C., Liu, M. & Neubig, R.R. Interdomain Interactions Regulate GDP Release from Heterotrimeric G Proteins. *Biochemistry* **38**, 13795-13800 (1999).
13. Wang, D. et al. A deep proteome and transcriptome abundance atlas of 29 healthy human tissues. in *Molecular systems biology* Vol. 15 e8503 (2019).

14. Itoh, H. et al. Presence of three distinct molecular species of Gi protein alpha subunit. Structure of rat cDNAs and human genomic DNAs. *Journal of Biological Chemistry* **263**, 6656-6664 (1988).
15. Linder, M.E., Ewald, D.A., Miller, R.J. & Gilman, A.G. Purification and characterization of Go alpha and three types of Gi alpha after expression in Escherichia coli. *Journal of Biological Chemistry* **265**, 8243-8251 (1990).
16. Taussig, R., Tang, W.J., Hepler, J.R. & Gilman, A.G. Distinct patterns of bidirectional regulation of mammalian adenylyl cyclases. *Journal of Biological Chemistry* **269**, 6093-6100 (1994).
17. Peleg, S., Varon, D., Ivanina, T., Dessauer, C.W. & Dascal, N. Gai Controls the Gating of the G Protein-Activated K<sup>+</sup> Channel, GIRK. *Neuron* **33**, 87-99 (2002).
18. Ivanina, T. et al. Gai1 and Gai3 Differentially Interact with, and Regulate, the G Protein-activated K<sup>+</sup> Channel. *Journal of Biological Chemistry* **279**, 17260-17268 (2004).
19. Rubinstein, M., Peleg, S., Berlin, S., Brass, D. & Dascal, N. Gai3 primes the G protein-activated K<sup>+</sup> channels for activation by coexpressed Gβγ in intact Xenopus oocytes. *The Journal of Physiology* **581**, 17-32 (2007).
20. Rubinstein, M. et al. Divergent regulation of GIRK1 and GIRK2 subunits of the neuronal G protein gated K<sup>+</sup> channel by GaiGDP and Gβγ. *The Journal of Physiology* **587**, 3473-3491 (2009).
21. Dizayee, S. et al. Galphai2- and Galphai3-specific regulation of voltage-dependent L-type calcium channels in cardiomyocytes. *PLoS One* **6**, e24979 (2011).
22. Cao, C. et al. Gai1 and Gai3 Are Required for Epidermal Growth Factor-Mediated Activation of the Akt-mTORC1 Pathway. *Science Signaling* **2**, ra17-ra17 (2009).
23. Köhler, D. et al. Gai2- and Gai3-Deficient Mice Display Opposite Severity of Myocardial Ischemia Reperfusion Injury. *PLOS ONE* **9**, e98325 (2014).
24. DeGeorge, B.R., Jr. et al. Targeted inhibition of cardiomyocyte Gi signaling enhances susceptibility to apoptotic cell death in response to ischemic stress. *Circulation* **117**, 1378-87 (2008).
25. Foerster, K. et al. Cardioprotection specific for the G protein Gai2 in chronic adrenergic signaling through β2-adrenoceptors. **100**, 14475-14480 (2003).
26. Kaur, K. et al. Gai2 signaling: friend or foe in cardiac injury and heart failure? *Naunyn Schmiedebergs Arch Pharmacol* **385**, 443-53 (2012).

27. Kuwano, Y., Adler, M., Zhang, H., Groisman, A. & Ley, K. Gai2 and Gai3 Differentially Regulate Arrest from Flow and Chemotaxis in Mouse Neutrophils. *The Journal of Immunology* **196**, 3828-3833 (2016).
28. Thompson, B.D. et al. Inhibition of Gai2 Activation by Gai3 in CXCR3-mediated Signaling. *Journal of Biological Chemistry* **282**, 9547-9555 (2007).
29. Chandan, N.R., Abraham, S., SenGupta, S., Parent, C.A. & Smrcka, A.V. A network of Gai signaling partners is revealed by proximity labeling proteomics analysis and includes PDZ-RhoGEF. *Science Signaling* **15**, eabi9869 (2022).
30. Masters, S.B. et al. Mutations in the GTP-binding site of G $\alpha$  alter stimulation of adenylyl cyclase. *Journal of Biological Chemistry* **264**, 15467-15474 (1989).
31. Graziano, M.P. & Gilman, A.G. Synthesis in Escherichia coli of GTPase-deficient mutants of G $\alpha$ . *Journal of Biological Chemistry* **264**, 15475-15482 (1989).
32. Wong, Y.H. et al. Mutant  $\alpha$  subunits of Gi2 inhibit cyclic AMP accumulation. *Nature* **351**, 63-65 (1991).
33. Dixon, A.S. et al. NanoLuc Complementation Reporter Optimized for Accurate Measurement of Protein Interactions in Cells. *ACS Chemical Biology* **11**, 400-408 (2016).
34. Laschet, C., Dupuis, N. & Hanson, J. A dynamic and screening-compatible nanoluciferase-based complementation assay enables profiling of individual GPCR-G protein interactions. *J Biol Chem* **294**, 4079-4090 (2019).
35. Kim, D.I. et al. An improved smaller biotin ligase for BioID proximity labeling. *Mol Biol Cell* **27**, 1188-96 (2016).
36. Chen, Z., Singer, W.D., Danesh, S.M., Sternweis, P.C. & Sprang, S.R. Recognition of the activated states of Galpha13 by the rgRGS domain of PDZRhoGEF. *Structure* **16**, 1532-43 (2008).
37. Li, Q. & Cerione, R.A. Communication between Switch II and Switch III of the Transducin  $\alpha$  Subunit Is Essential for Target Activation. *Journal of Biological Chemistry* **272**, 21673-21676 (1997).
38. Pereira, R. & Cerione, R.A. A Switch 3 Point Mutation in the  $\alpha$  Subunit of Transducin Yields a Unique Dominant-negative Inhibitor. *Journal of Biological Chemistry* **280**, 35696-35703 (2005).
39. Grishina, G. & Berlot, C.H. Mutations at the Domain Interface of G $\alpha$  Impair Receptor-mediated Activation by Altering Receptor and Guanine Nucleotide Binding. *Journal of Biological Chemistry* **273**, 15053-15060 (1998).



40. Kim, H.R., Ahn, D., Jo, J.B. & Chung, K.Y. Effect of  $\alpha$ -helical domain of Gi/o  $\alpha$  subunit on GDP/GTP turnover. *Biochemical Journal* **479**, 1843-1855 (2022).
41. Jones, J.C., Jones, A.M., Temple, B.R.S. & Dohlman, H.G. Differences in intradomain and interdomain motion confer distinct activation properties to structurally similar G $\alpha$  proteins. *Proceedings of the National Academy of Sciences* **109**, 7275-7279 (2012).
42. Marin, E.P. et al. The Function of Interdomain Interactions in Controlling Nucleotide Exchange Rates in Transducin. *Journal of Biological Chemistry* **276**, 23873-23880 (2001).
43. Toyama, Y. et al. Dynamic regulation of GDP binding to G proteins revealed by magnetic field-dependent NMR relaxation analyses. *Nature Communications* **8**, 14523 (2017).
44. Noel, J.P., Hamm, H.E. & Sigler, P.B. The 2.2 Å crystal structure of transducin- $\alpha$  complexed with GTP $\gamma$ S. *Nature* **366**, 654-663 (1993).
45. Codina, J. & Birnbaumer, L. Requirement for intramolecular domain interaction in activation of G protein alpha subunit by aluminum fluoride and GDP but not by GTP gamma S. *Journal of Biological Chemistry* **269**, 29339-29342 (1994).
46. Marsh, S.R., Grishina, G., Wilson, P.T. & Berlot, C.H. Receptor-Mediated Activation of G $\alpha$ : Evidence for Intramolecular Signal Transduction. *Molecular Pharmacology* **53**, 981-990 (1998).
47. Tesmer, J.J.G., Sunahara, R.K., Gilman, A.G. & Sprang, S.R. Crystal Structure of the Catalytic Domains of Adenylyl Cyclase in a Complex with G $\alpha$ -GTP $\gamma$ S. *Science* **278**, 1907-1916 (1997).
48. Tesmer, V.M., Kawano, T., Shankaranarayanan, A., Kozasa, T. & Tesmer, J.J.G. Snapshot of Activated G Proteins at the Membrane: The G $\alpha$ q-GRK2-G $\beta$  $\gamma$  Complex. *Science* **310**, 1686-1690 (2005).
49. Lyon, A.M., Dutta, S., Boguth, C.A., Skiniotis, G. & Tesmer, J.J.G. Full-length G $\alpha$ q-phospholipase C- $\beta$ 3 structure reveals interfaces of the C-terminal coiled-coil domain. *Nature Structural & Molecular Biology* **20**, 355-362 (2013).
50. Hajicek, N. et al. Identification of critical residues in G( $\alpha$ )13 for stimulation of p115RhoGEF activity and the structure of the G( $\alpha$ )13-p115RhoGEF regulator of G protein signaling homology (RH) domain complex. *J Biol Chem* **286**, 20625-36 (2011).
51. Slep, K.C. et al. Structural determinants for regulation of phosphodiesterase by a G protein at 2.0 Å. *Nature* **409**, 1071-1077 (2001).

52. Day, P.W. et al. Characterization of the GRK2 binding site of Galphaq. *J Biol Chem* **279**, 53643-52 (2004).
53. Liu, W. & Northup, J.K. The helical domain of a G protein alpha subunit is a regulator of its effector. *Proc Natl Acad Sci U S A* **95**, 12878-83 (1998).
54. Gao, Y. et al. Structure of the Visual Signaling Complex between Transducin and Phosphodiesterase 6. *Mol Cell* **80**, 237-245 e4 (2020).
55. Pero, R.S. et al.  $G\alpha_{i2}$ -mediated signaling events in the endothelium are involved in controlling leukocyte extravasation. *Proceedings of the National Academy of Sciences* **104**, 4371-4376 (2007).
56. Surve, C.R., To, J.Y., Malik, S., Kim, M. & Smrcka, A.V. Dynamic regulation of neutrophil polarity and migration by the heterotrimeric G protein subunits Galphai-GTP and Gbetagamma. *Sci Signal* **9**, ra22 (2016).
57. Nobles, M., Montaigne, D., Sebastian, S., Birnbaumer, L. & Tinker, A. Differential effects of inhibitory G protein isoforms on G protein-gated inwardly rectifying K<sup>+</sup> currents in adult murine atria. *American Journal of Physiology-Cell Physiology* **314**, C616-C626 (2018).
58. Mumby, S.M. & Gilman, A.G. Synthetic peptide antisera with determined specificity for G protein alpha or beta subunits. *Methods Enzymol* **195**, 215-33 (1991).
59. McAlister, G.C. et al. MultiNotch MS3 Enables Accurate, Sensitive, and Multiplexed Detection of Differential Expression across Cancer Cell Line Proteomes. *Analytical Chemistry* **86**, 7150-7158 (2014).
60. Jo, S., Kim, T., Iyer, V.G. & Im, W. CHARMM-GUI: a web-based graphical user interface for CHARMM. *J Comput Chem* **29**, 1859-65 (2008).
61. Hess, B., Kutzner, C., van der Spoel, D. & Lindahl, E. GROMACS 4: Algorithms for Highly Efficient, Load-Balanced, and Scalable Molecular Simulation. *J Chem Theory Comput* **4**, 435-47 (2008).
62. Huang, J. et al. CHARMM36m: an improved force field for folded and intrinsically disordered proteins. *Nat Methods* **14**, 71-73 (2017).
63. Berendsen, H.J.C.P., J.P.M.; van Gunsteren, W.F.; DiNola, A.; Haak, J.R. Molecular dynamics with coupling to an external bath. *The Journal of Chemical Physics* **81**, 3684-3690 (1984).
64. Andersen, H.C. Rattle: A “velocity” version of the shake algorithm for molecular dynamics calculations. *Journal of Computational Physics* **52**, 24-34 (1983).

65. T. Darden, D.Y., L. Pedersen. Particle mesh Ewald: An  $N \cdot \log(N)$  method for Ewald sums in large systems. *Journal of Chemical Physics* **98**, 10089–10092 (1993).
66. Evans, D.J.H., B.L. The Nose–Hoover thermostat. *The Journal of Chemical Physics* **83**, 4069-4074 (1985).
67. Parrinello, M.R., A. Polymorphic transitions in single crystals: A new molecular dynamics method. *Journal of Applied Physics* **52**, 7182-7190 (1981).
68. Petrova, S.S.S.e., A.D. The Origin of the Method of Steepest Descent. *Historia Mathematica* **24**, 361-375 (1997).
69. Gogoshin, G.B., E.; Rodin, A.S. New Algorithm and Software (BNOmics) for Inferring and Visualizing Bayesian Networks from Heterogeneous Big Biological and Genetic Data. *Journal of Computational Biology* **24**, 340-356 (2017).

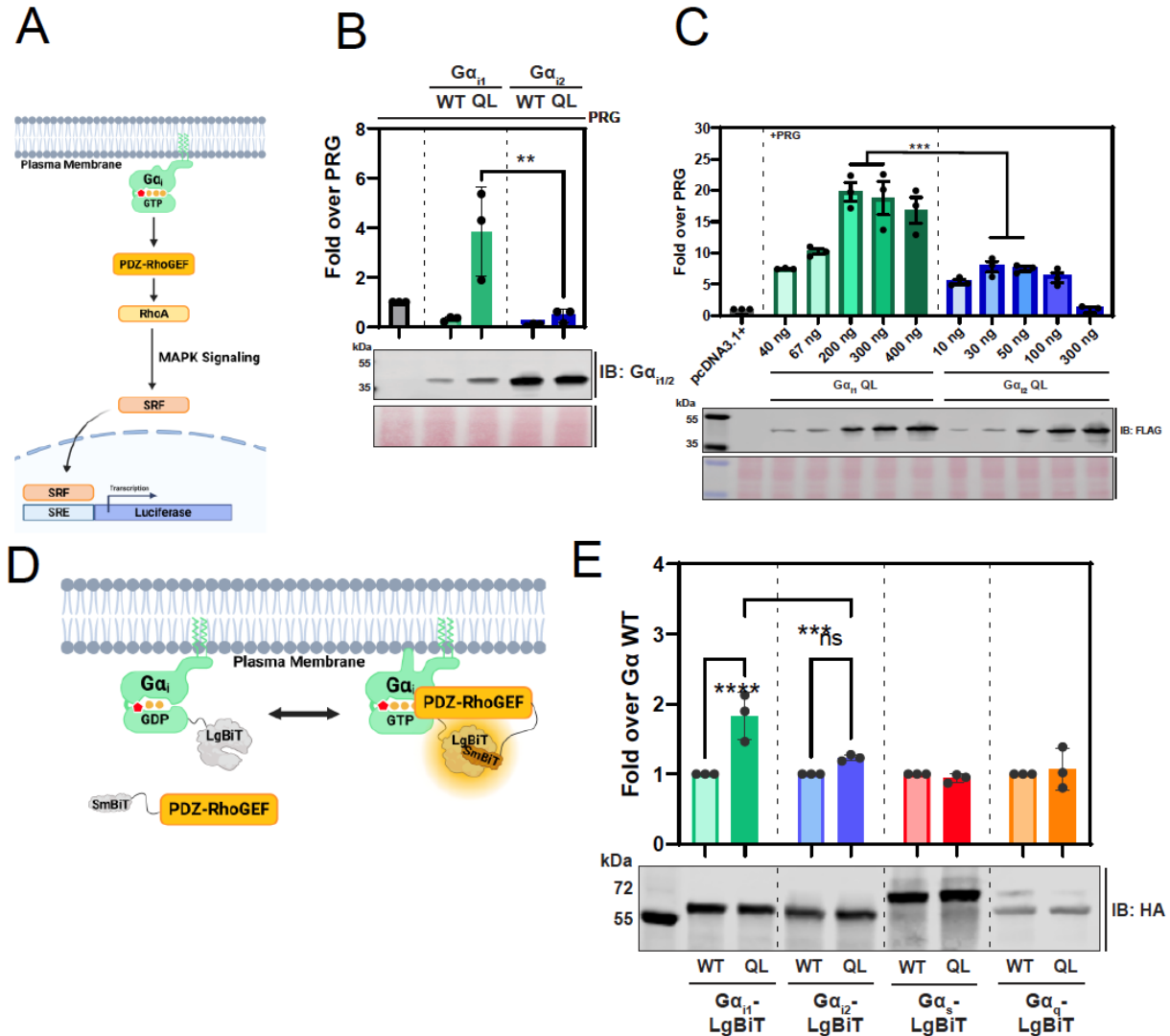


**Figure 1.** G $\alpha_{i1}$  more efficiently interacts with PRG than G $\alpha_{i2}$ .

**A)** Diagram of the SRE luciferase used to assess G $\alpha$  regulation of PRG. HEK293 cells were co-transfected with control plasmid pcDNA 3.1 or G $\alpha$  plasmids as indicated, PRG, and an SRE luciferase reporter plasmid. 24 h after transfection One-Glo luciferase reagent was added and luminescence was measured using a plate reader.

**B)** Comparison of G $\alpha_{i1}$  and G $\alpha_{i2}$  which were transfected as indicated. All wells were transfected with PRG. Fold over PRG was calculated as the luminescent signal with G $\alpha$  subunits co-transfected with PRG divided by the signal with PRG co transfected with control pcDNA 3.1 plasmid.

**C)** Cells were transfected with the indicated amount of FLAG-G $\alpha_{i1}$  QL or FLAG-G $\alpha_{i2}$  QL adjusted to achieve equivalent expression as shown in the flag western blot shown in the bottom panel. To calculate the significance in the difference in maximal stimulation the values for 200 and 300 ng of G $\alpha_{i1}$  plasmid were averaged and compared to the average of the 30 and 50 ng values for G $\alpha_{i2}$ . T-test \*\*\* P<0.001.

**D)** Diagram of the  $G\alpha_i$ -LgBiT complementation assay used with  $G\alpha_i$  fused to LgBiT and PRG with N-terminal fusion of SmBiT peptide natural peptide sequence (PRG-SmBiT).

**E)** The indicated plasmids were co-transfected into HEK293 cells with PRG-SmBiT. 24 h after transfection cells were transferred into a 96 well plate and furimazine substrate was added for 15 min prior to measurement of luminescence in a plate reader.

All experiments were performed with at least three biological replicates of assays performed in triplicate. Unless otherwise indicated data was analyzed with a one-way ANOVA with a Šídák post-test. \*\*  $P < 0.01$  and \*\*\*\*  $P < .0001$ .

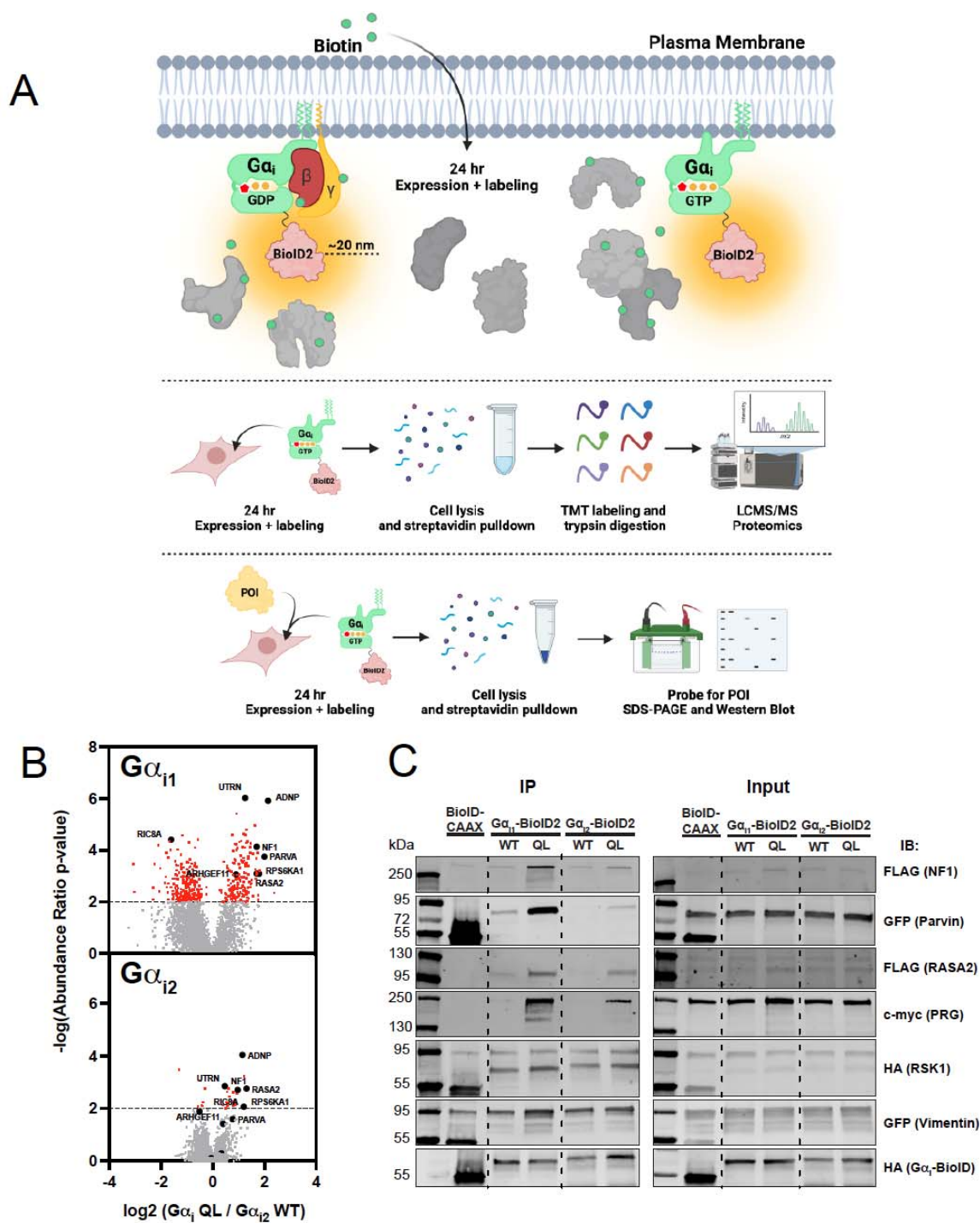


**Figure 2.** Active  $G\alpha_{i2}$  weakly engages the proximity interactome relative to  $G\alpha_{i2}$ .

**A)** Experimental outline for biotin proximity labeling assays.

**B)** The indicated HA- $G\alpha_i$ -BioID2 constructs were transiently transfected into HT1080 cells, in triplicate for each condition for 24 h followed by isolation of biotinylated proteins and analysis by TMT Mass Spectrometry. To control for differences in overall biotinylation each sample was normalized based on the total spectral counts for all of the proteins identified (~4000 proteins). Spectral counts were then analyzed as the ratio

of samples transfected with the  $G\alpha_i$ -QL plasmids relative to samples transfected with  $G\alpha_{i2}$  WT. The dashed line indicates a p value of 0.01 and all statistically significant proteins are colored in red.

**C)** The indicated  $G\alpha_i$ -BioID2 constructs were co-transfected with the indicated epitope-tagged protein into HEK293 cells. 24 h after transfection biotinylated proteins were isolated with streptavidin beads and the followed by western blotting to determine the amount of biotinylated target protein pulled down. Shown is a representative western blot of an experiment performed twice.

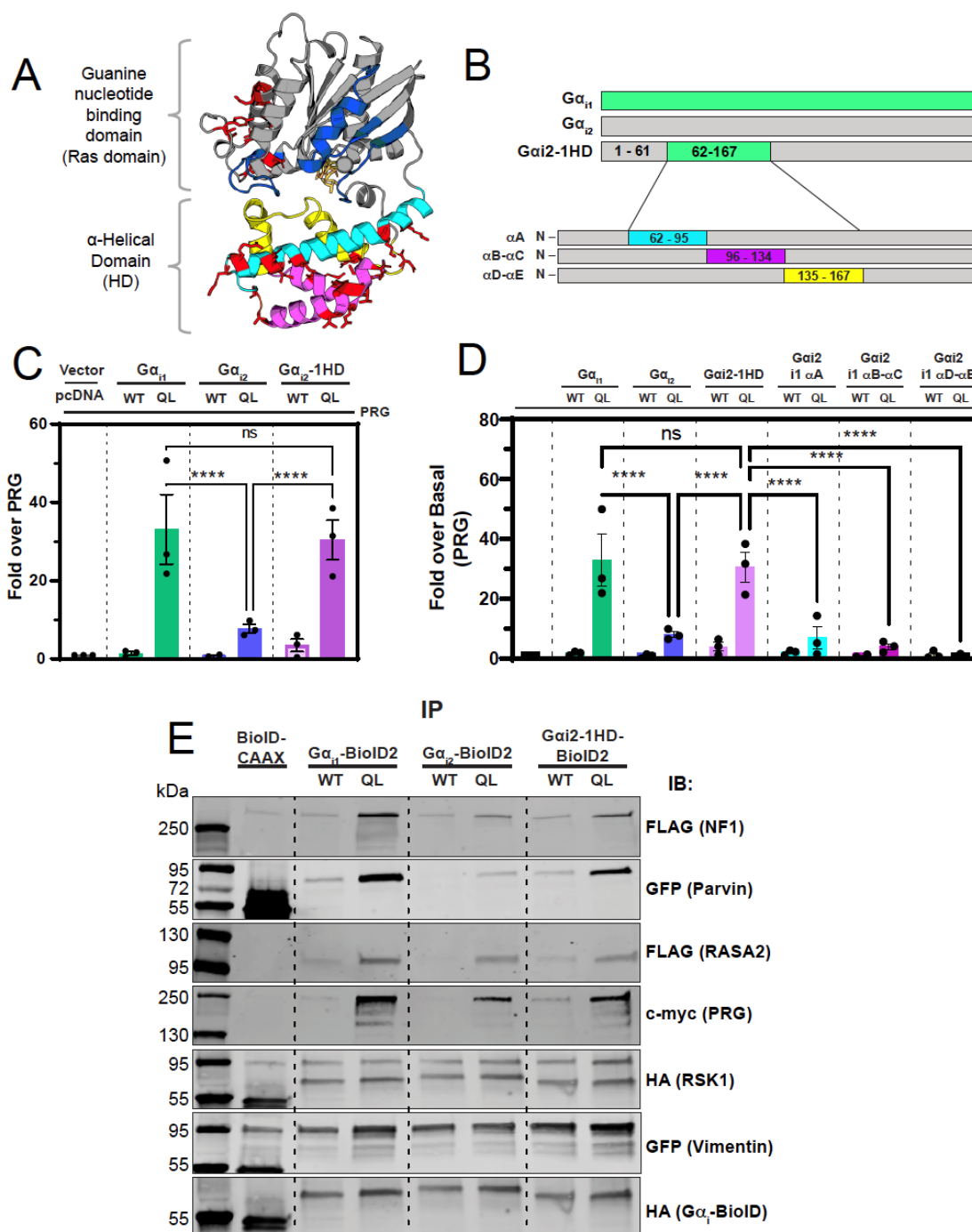


**Figure 3.** Substitution of the  $G\alpha_{i1}$  helical domain into  $G\alpha_{i2}$  partially restores activation of PRG and proximity proteome engagement.

**A)** Diagrammatic representation of the  $G\alpha_{i1}$  structure. In cyan, magenta, and yellow are subdivisions of the helical domain. Switch I-III are in blue. Red stick amino acids are amino acids conserved between  $G\alpha_{i1}$  and  $G\alpha_{i3}$  but not  $G\alpha_{i2}$ . PDB: 1CIP.

**B)** Diagram of the constructs used in these experiments.



**C) and D)** The indicated constructs were co-transfected with PRG and SRE-Luc and the assay was performed as in Fig. 1. Western blots for expression and cAMP assays are in Fig. S1 A,B,C and D. E)

**E)** The indicated  $G\alpha_i$  constructs were co-transfected into HEK293 cells with the indicated epitope tagged constructs and analyzed as in Fig. 2B. The  $G\alpha_{i1}$  and  $G\alpha_{i2}$  western blots are the same as in Fig. 2E with  $G\alpha_{i2}$ -1HD added for comparison. Shown is a representative western blot of an experiment performed twice. The input western blot is in Fig. S1E. All SRE-luc experiments were performed with 3 biological replicates performed in triplicate. Data are  $\pm$ -SEM analyzed by One-way ANOVA with Šídák post-test. \*\*\*\*  $P < 0.0001$ .

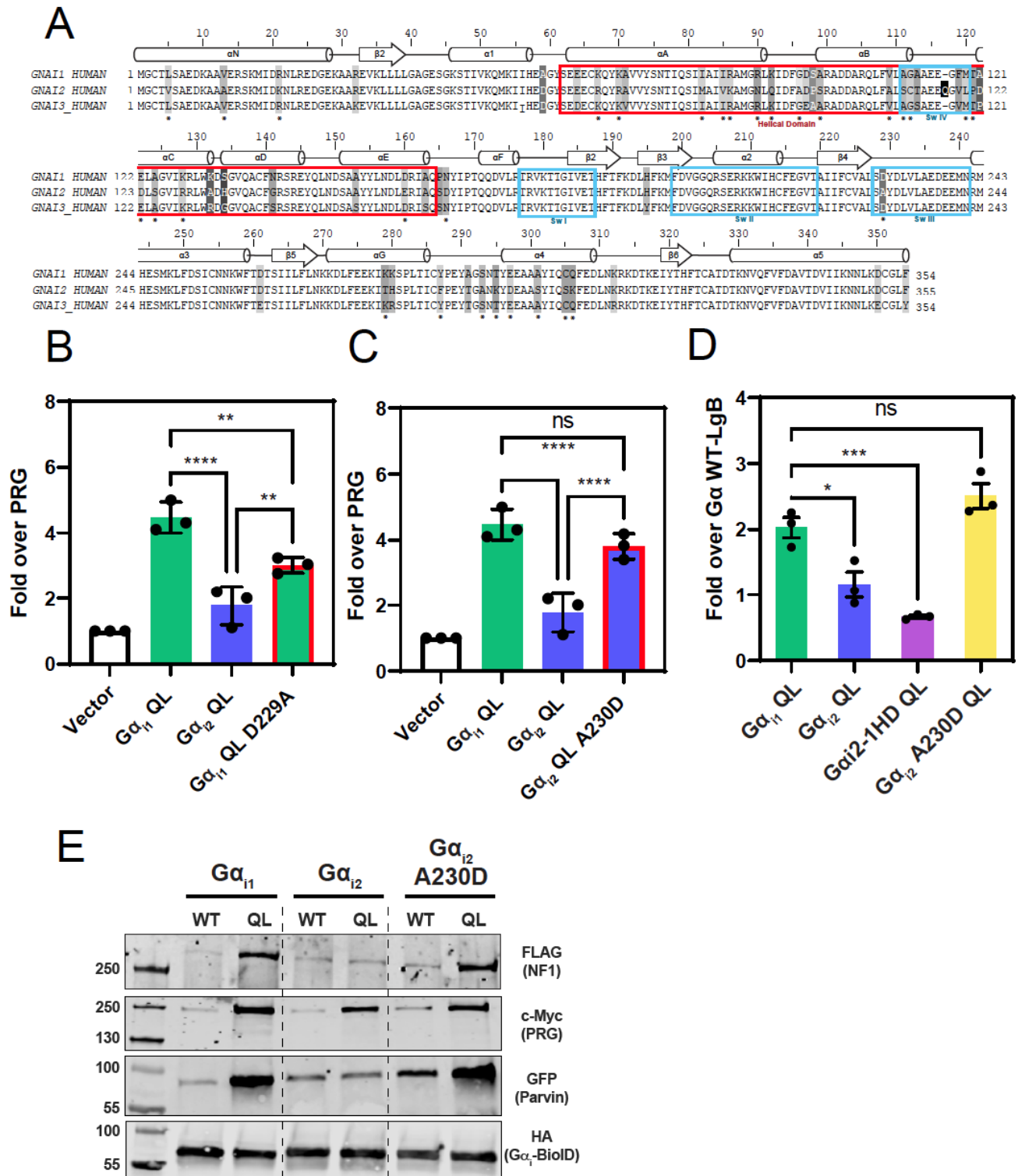


**Figure 4.**  $G\alpha_{11}$  D229/ $G\alpha_{12}$  A230<sup>s4h3.3</sup> in the Ras-like domain is critical for differences in PRG activation.

- A)** Alignment of human  $G\alpha_{i1}$ ,  $G\alpha_{i2}$ , and  $G\alpha_{i3}$ . Boxed in blue are the  $G\alpha_i$  switch regions. The helical domain is boxed in red. Starred (\*) amino acids are identical in  $G\alpha_{i1}$  and  $G\alpha_{i3}$  but different in  $G\alpha_{i2}$ .
- B)** Mutation of  $G\alpha_{i1}$  D229<sup>s4h3.3</sup> to the corresponding A in  $G\alpha_{i2}$  (A230<sup>s4h3.3</sup>) reduces the ability to activate PRG.
- C)** Mutation of  $G\alpha_{i2}$  A230 to the corresponding D in  $G\alpha_{i1}$  (D229) enhances the ability of  $G\alpha_{i2}$  to activate PRG.
- D)** Mutation of  $G\alpha_{i2}$  A230 to the corresponding D in  $G\alpha_{i1}$  (D229) enhances interactions between  $G\alpha_{i2}$ -LgBiT and PRG-SmBiT in the luciferase complementation assay.
- E)** Mutation of  $G\alpha_{i2}$  A230 to the corresponding D in  $G\alpha_{i1}$  (D229) enhances interactions with other proteins in the  $G\alpha_i$  proximity interactome. Shown is representative western blot for an experiment performed twice. All SRE-luc and complementation experiments were performed with 3 biological replicates performed in triplicate. Data are +/- SEM analyzed by One-way ANOVA with Šídák post-test; \*  $P < 0.05$ , \*\*  $P < 0.01$ , \*\*\*  $P < 0.001$ , \*\*\*\*  $P < 0.0001$ .

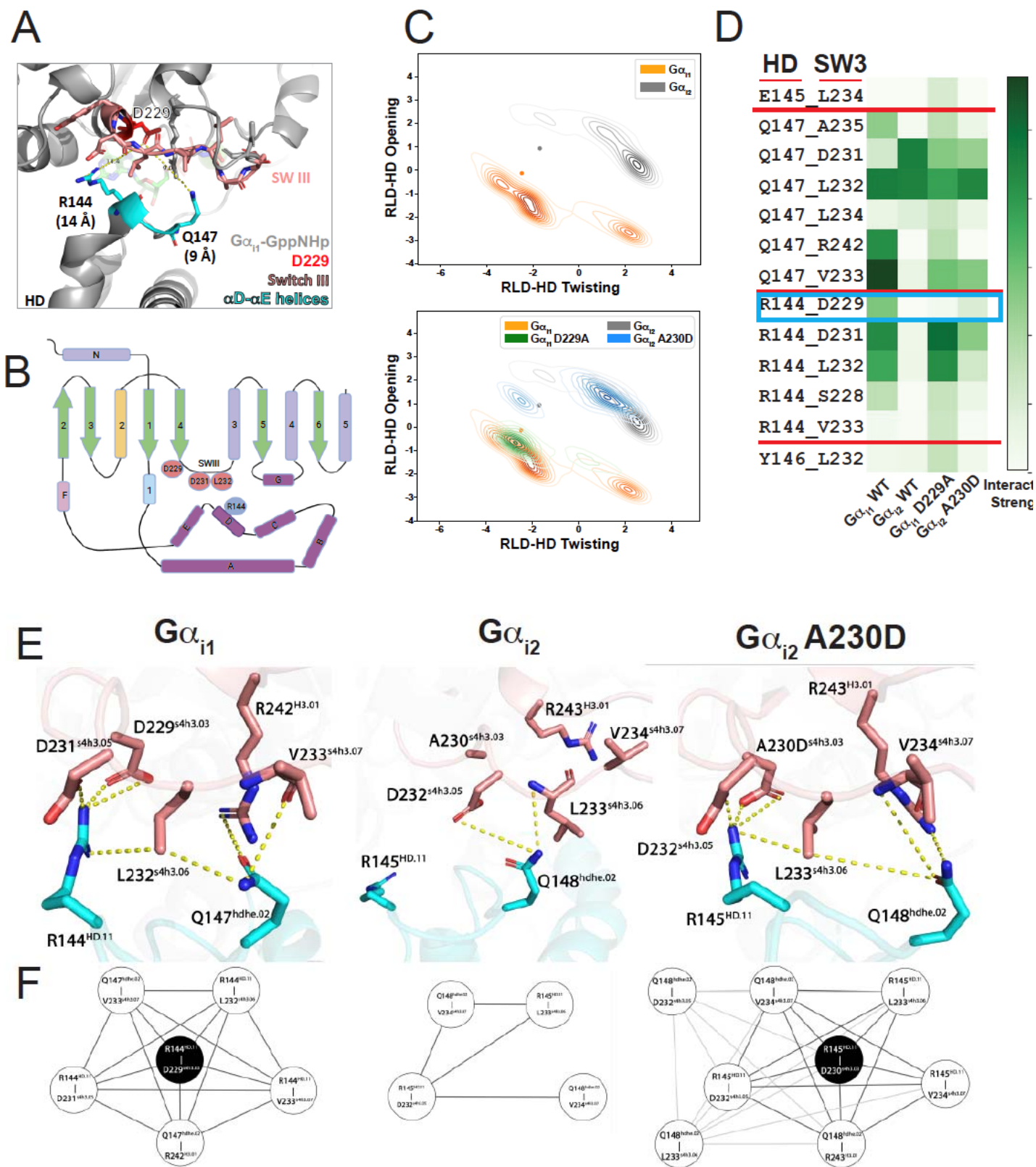


**Figure 5. Molecular dynamics simulations and Bayesian network analysis reveal an interaction network that is not apparent in three dimensional crystal structures in the GTP bound state.**

**A)** Diagram of a structure of  $G\alpha_{i1}$ -GTP showing the distance between D229 and the nearest HD residues.

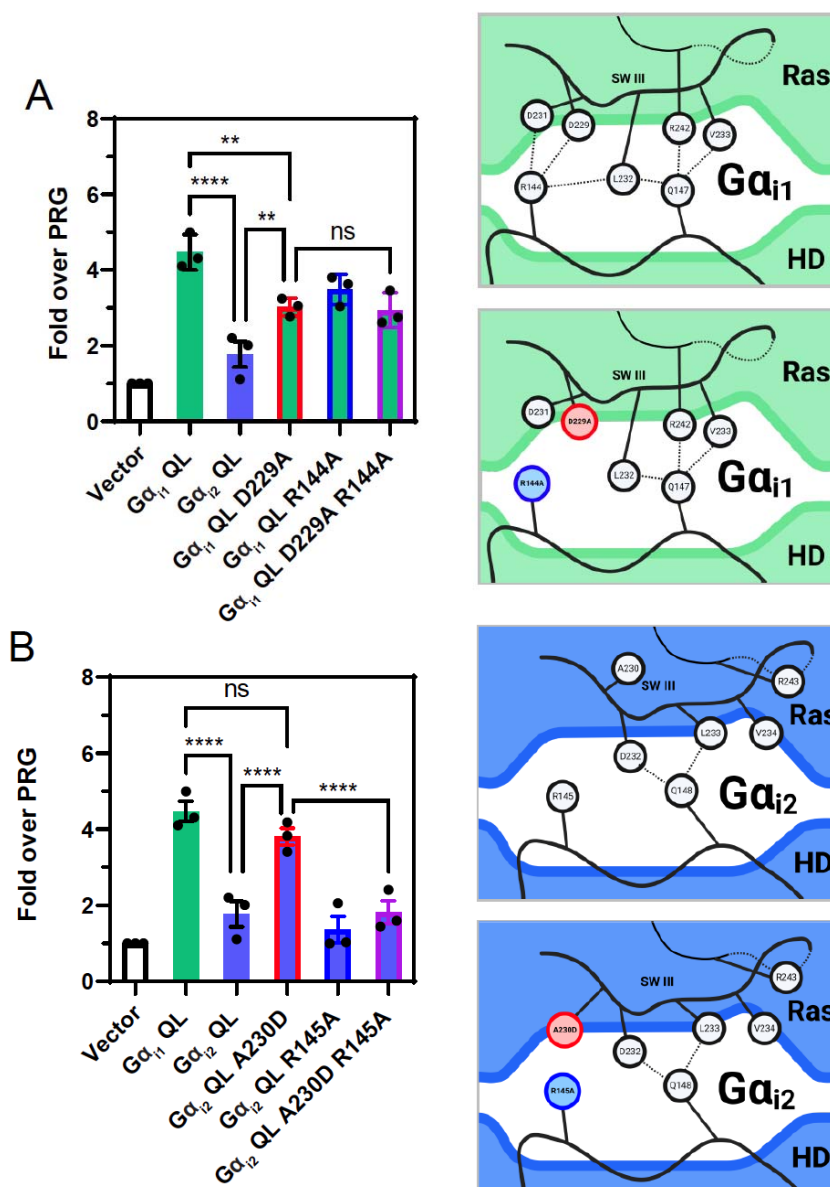
**B)** Ribbon representation of  $G\alpha$  subunit structure highlighting key amino acids at the Switch III-helical domain interface.

**C)** Principal component analysis of  $G\alpha_{i1}$ -GTP vs.  $G\alpha_{i2}$ -GTP.

**D)** Interaction frequency heat map of amino acid interactions between Switch III amino acids and amino acids in the HD comparing the GTP bound states of  $G\alpha_{i1}$ ,  $G\alpha_{i2}$ ,  $G\alpha_{i1}$  D229A, and  $G\alpha_{i2}$  A230D.

**E)** Diagram of interdomain interactions involving D229 in  $G\alpha_{i1}$ -GTP (top panel) and A230 in  $G\alpha_{i2}$ -GTP (middle panel) and  $G\alpha_{i2}$ -GTP A230D (right panel).

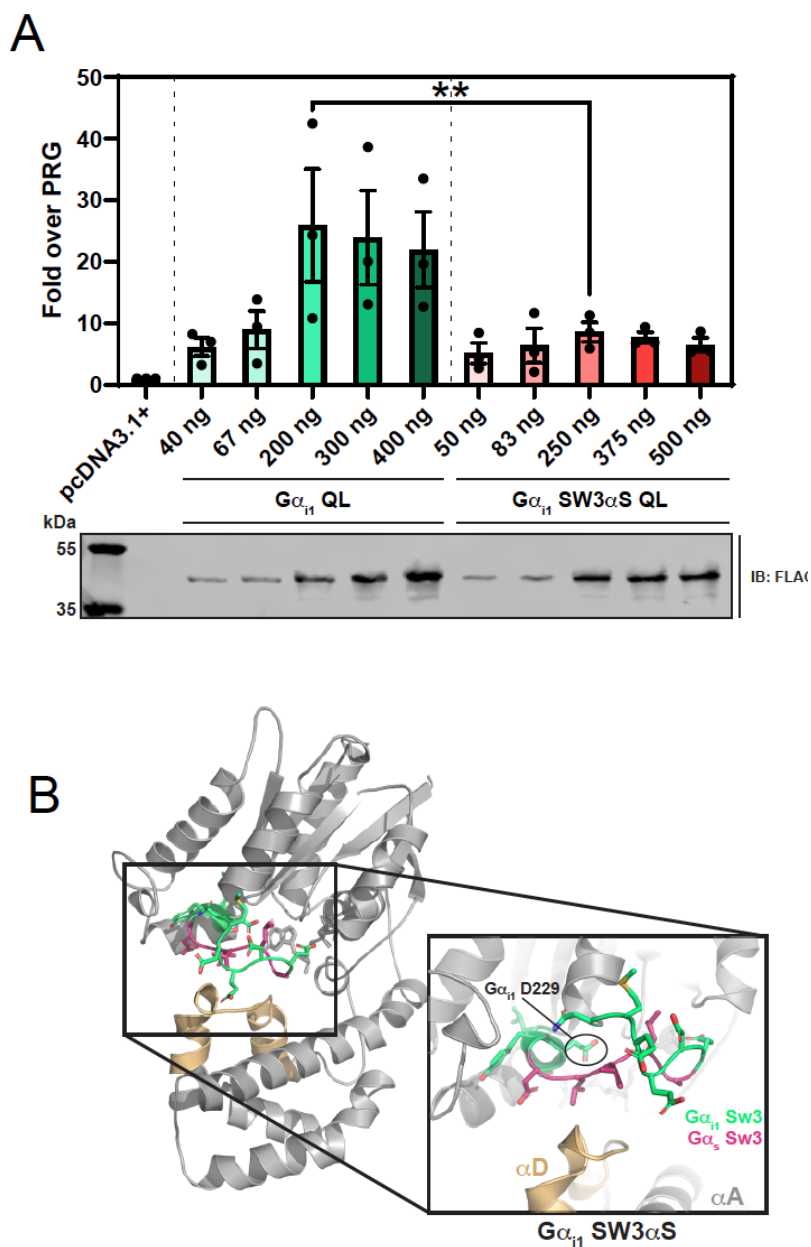
**F)** Bayesian networks showing interdomain interactions driven by D229 and HD R144 in  $G\alpha_{i1}$ -GTP(left panel), In  $G\alpha_{i2}$  A230 cannot interact with R145 weakening the overall interaction network (middle panel), Substitution of D for A230 in  $G\alpha_{i2}$ -GTP leads to interactions with R145 stabilizing the interaction network between the HD and Switch III. Each node represents a contact made between the HD and Switch III, the thickness of the edge connecting the nodes indicates whether the edge was present in the  $G\alpha_{i1}$  network.



**Figure 6.**  $G\alpha_{i1}$  D229/ $G\alpha_{i2}$  A230 controls HD-RLD interdomain interactions.

**A)** SRE luciferase assay showing PRG activation by QL versions of  $G\alpha_{i1}$ ,  $G\alpha_{i2}$ ,  $G\alpha_{i1}$  D229A,  $G\alpha_{i1}$  R144A, and  $G\alpha_{i1}$  D229A-R144A (left panel). The top right panel is a diagram of the WT  $G\alpha_{i1}$  interaction network. The bottom right panel is a diagram of the  $G\alpha_{i1}$  interaction network indicating the amino acid substitutions in red and blue.

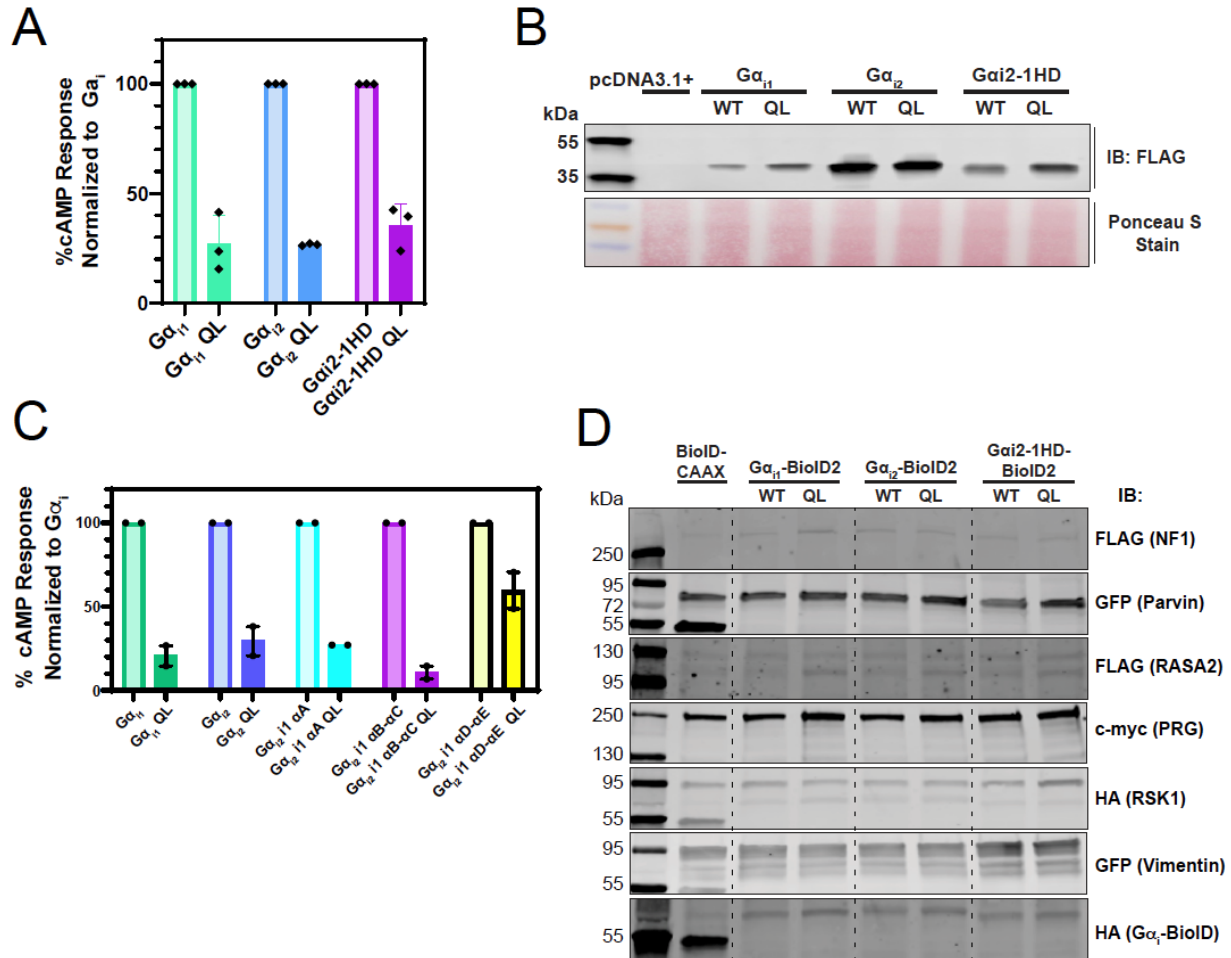
**B)** SRE luciferase assay showing PRG activation by QL versions of  $G\alpha_{i1}$ ,  $G\alpha_{i2}$ ,  $G\alpha_{i2}$  A230D,  $G\alpha_{i2}$  R145A, and  $G\alpha_{i2}$  A230D-R145A. The top right panel is a diagram of the WT  $G\alpha_{i2}$  interaction network. The bottom right panel is a diagram of the  $G\alpha_{i2}$  interaction network indicating the amino acid substitutions in red and blue. Experiments were performed with 3 biological replicates performed in triplicate. Data are +/- SEM analyzed by One-way ANOVA with Šídák post-test; \*  $P < 0.05$ , \*\*  $P < 0.01$ , \*\*\*  $P < 0.001$ , \*\*\*\*  $P < 0.0001$ .



**Figure 7.  $G\alpha_{i1}$  Switch III is critical for activation of PRG.**

**A)** Switch III amino acids in  $G\alpha_{i1}$  were substituted with the cognate amino acids in  $G\alpha_s$  and assayed for PRG activation using the SRE-luc assay. Experiments were performed with 3 biological replicates performed in duplicate. Data are +/- SEM analyzed by One-way ANOVA with Šídák post-test; \*  $P < 0.05$ , \*\*  $P < 0.01$ , \*\*\*  $P < 0.001$ , \*\*\*\*  $P < 0.0001$ .

**B)** Structural representation of active  $G\alpha_{i1}$  and active  $G\alpha_{i1}$  with  $G\alpha_s$  substitutions made in  $G\alpha_{i1}$  Switch III.  $G\alpha_{i1}$  is grey, the  $\alpha D$  helix in the HD is shown in tan for orientation,  $G\alpha_{i1}$  Switch III residues are shown in green sticks, and the  $G\alpha_{i1}$  residues mutated to corresponding residues in  $G\alpha_s$  are in pink. PDB ID: 1CIP.





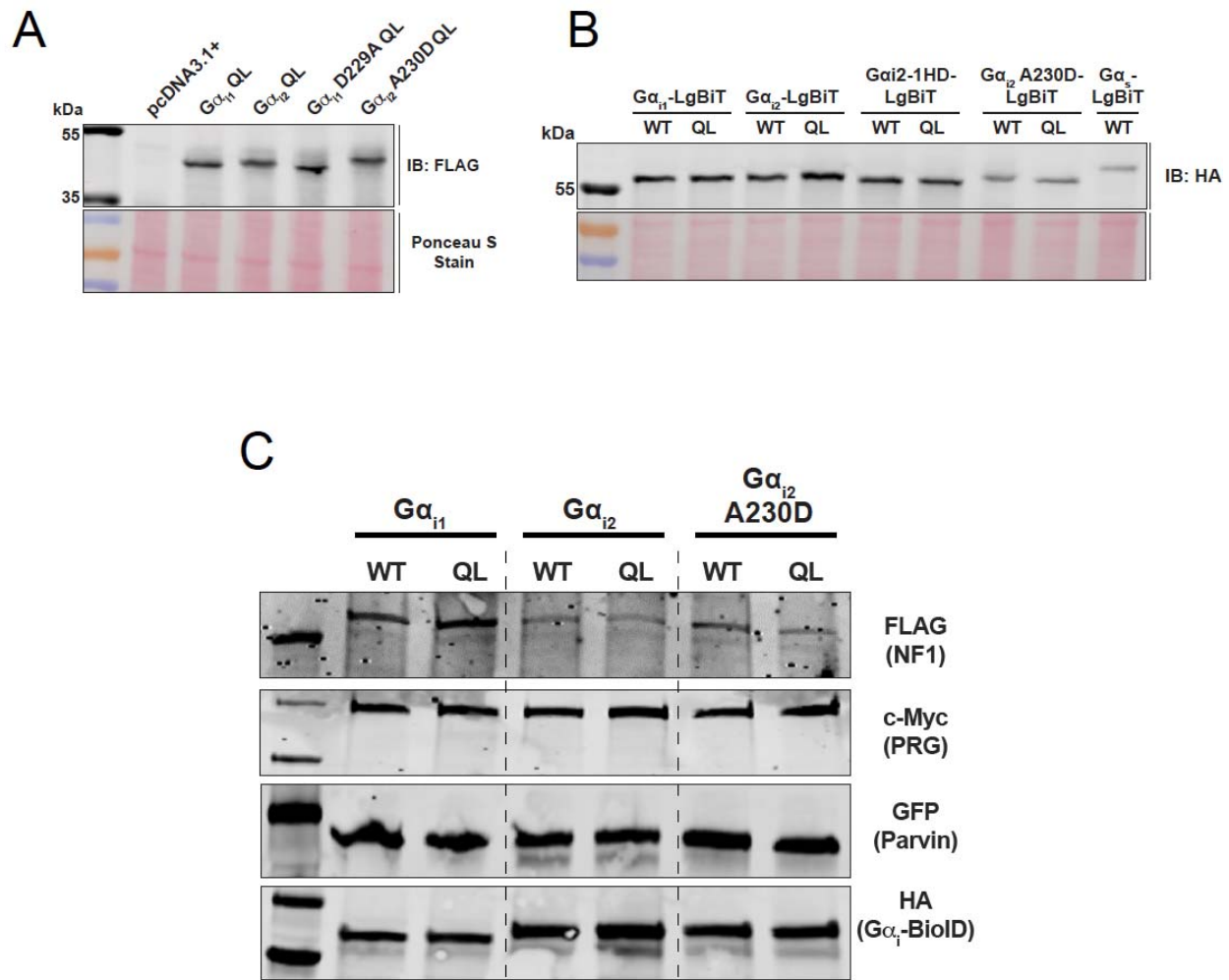


**Figure S2.** Supporting data for figure 4. A) Western blot for proteins used in Fig. 4B and C. B) Western blot for proteins used in Fig. 4D. C) Input western blots for BioID2 experiments in Fig. 4E.

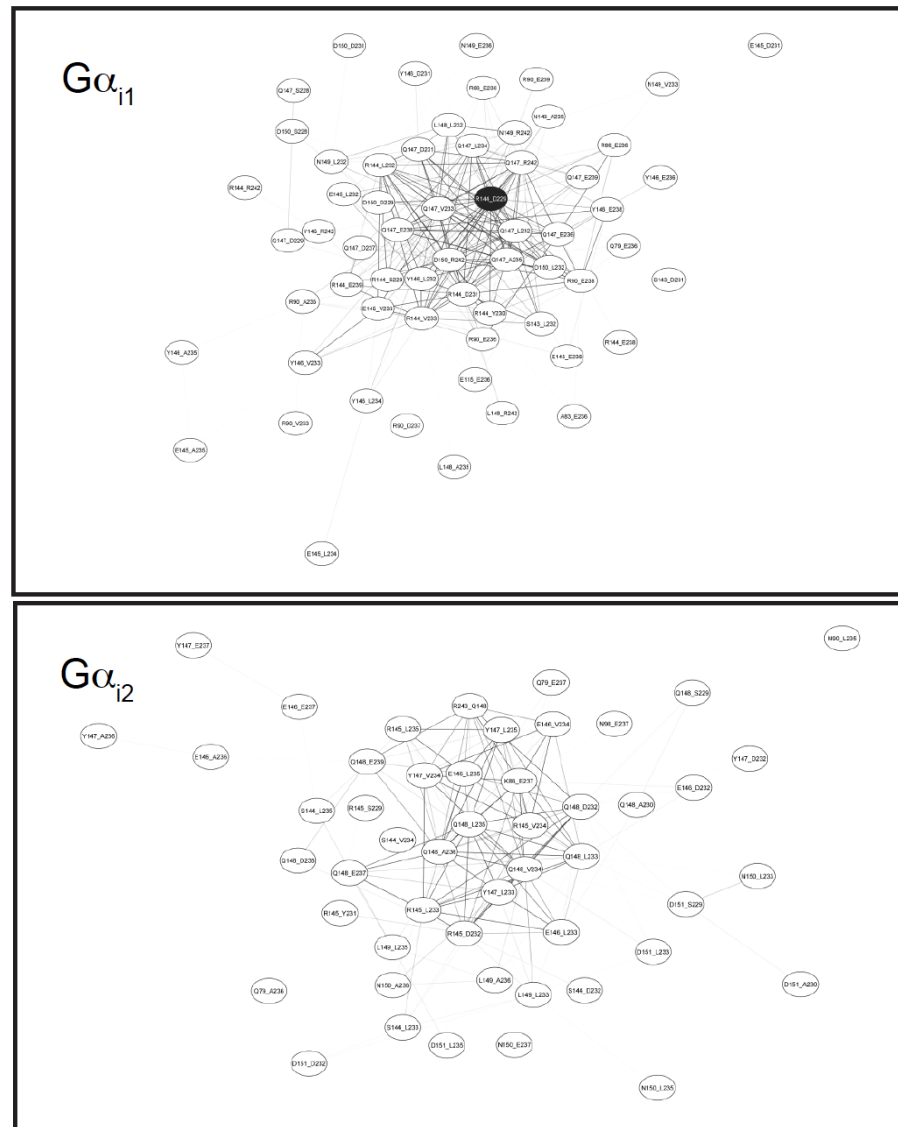


**Figure S3.** Full Bayesian networks for  $G_{\alpha_{i1}}$  and  $G_{\alpha_{i2}}$  supporting figure 5.

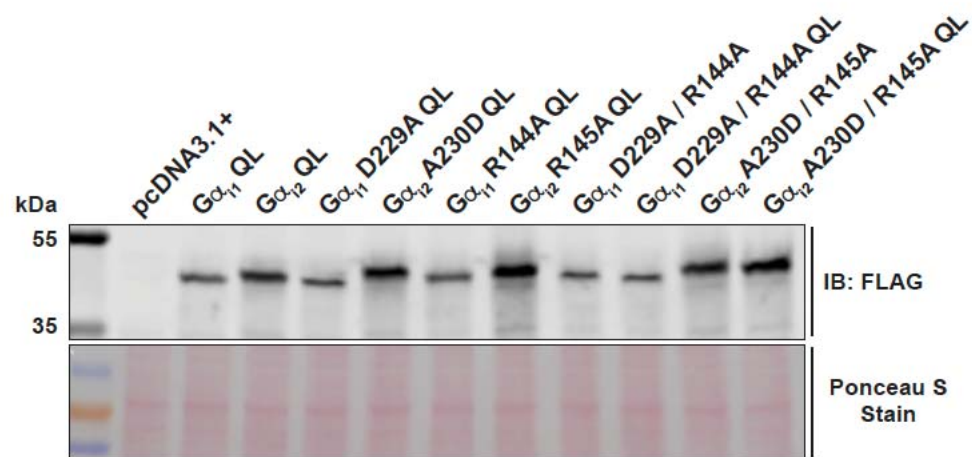


**Figure S4.** Supporting data for Figure 6. A) Western blot for protein expression for Fig. 6A and B.

	HD.11	s4h3.3	
GNAS2	N		S
GNAL	N		S
GNAI1	R	—	D
GNAI2	R		A
GNAI3	R	—	D
GNAT1	S		A
GNAT2	A		A
GNAT3	S		A
GNAO	R		G
GNAZ	S		G
GNAQ	R	—	E
GNA11	R	—	E
GNA14	R	—	E
GNA15	R	—	E
GNA12	S		E
GNA13	R	—	E

Aliphatic/hydrophobic	ILVAM
Aromatic	FWY
Positive	KRH
Negative	DE
Hydrophilic	STNQ
Conformationally Special	PG
Cysteine	C

**Figure S5.** Alignments of all the G protein  $\alpha$  subunit families highlighting the presence or absence of ionic lock amino acids HD.11 in the helical domain and s4h3.3 in the RLD